CLIMATOLOGY

Early sea ice decline off East Antarctica at the last glacial–interglacial climate transition

Henrik Sadatzki[1]*†, Bradley Opdyke[2], Laurie Menviel[3,4], Amy Leventer[5], Janet M. Hope[2], Jochen J. Brocks[2], Stewart Fallon[2], Alexandra L. Post[6], Philip E. O'Brien[2], Katharine Grant[2], Leanne Armand[2]‡

Antarctic climate warming and atmospheric CO_2 rise during the last deglaciation may be attributed in part to sea ice reduction in the Southern Ocean. Yet, glacial–interglacial Antarctic sea ice dynamics and underlying mechanisms are poorly constrained, as robust sea ice proxy evidence is sparse. Here, we present a molecular biomarker-based sea ice record that resolves the spring/summer sea ice variability off East Antarctica during the past 40 thousand years (ka). Our results indicate that substantial sea ice reduction culminated rapidly and contemporaneously with upwelling of carbon-enriched waters in the Southern Ocean at the onset of the last deglaciation but began at least ~2 ka earlier probably driven by an increasing local integrated summer insolation. Our findings suggest that sea ice reduction and associated feedbacks facilitated stratification breakup and outgassing of CO_2 in the Southern Ocean and warming in Antarctica but may also have played a leading role in initializing these deglacial processes in the Southern Hemisphere.

INTRODUCTION

Ice core records reveal that the last deglaciation was marked by a warming over Antarctica of ~8°C and concomitant atmospheric CO_2 rise of ~80 ppmv between ~17.5 and ~11.7 thousand years (ka) ago (*1*–*3*). The deglacial Antarctic warming and atmospheric CO_2 rise were interrupted by a millennial-scale cooling event that is referred to as the Antarctic Cold Reversal (ACR) and coincided with stagnant atmospheric CO_2 (*1*, *2*). The close link between Antarctic climate and atmospheric CO_2 on orbital and millennial time scales suggests that processes in the Southern Ocean were instrumental in driving deglacial changes in atmospheric CO_2 and thus global climate (*1*). In particular, breakup of the glacial deep stratification and invigoration of overturning in the Southern Ocean are widely believed to have led to outgassing of deeply sequestered CO_2 to the atmosphere in two major pulses during the last deglaciation (*4*–*7*). It has been proposed that the glacial deep stratification in the Southern Ocean and deep-ocean carbon storage may have been dynamically linked with an expansion of (summer) sea ice around Antarctica, while deglacial breakup of that stratification was probably coupled with sea ice reduction (*4*, *8*–*10*). A reduction of the glacial Antarctic sea ice cover would have increased the sea-air gas and heat exchange and lowered the albedo, thus forming a critical mechanism facilitating both enhanced outgassing of CO_2 from the Southern Ocean and Antarctic warming (*11*).

The deglacial phases of warming across Antarctica and atmospheric CO_2 rise were coincident with major reductions in the Atlantic Meridional Overturning Circulation (AMOC) and Northern Hemisphere cold spells during Heinrich Stadial 1 [~17.5 to 14.7 ka ago; following Barker *et al.* (*12*) and Rasmussen *et al.* (*13*), we use the term "Heinrich Stadial 1" to denote Greenland Stadial 2.1a that contains but is not equivalent to Heinrich event 1] and the Younger Dryas [~12.9 to 11.7 ka ago; corresponding to Greenland Stadial 1 (*13*)] (*7*, *14*). In accordance with the conceptual model of the "thermal bipolar seesaw" (*15*), model simulations show that AMOC reductions forced by freshwater input to the North Atlantic can be accompanied by invigoration of Southern Ocean overturning, reduction of the Antarctic sea ice cover, and Southern Hemisphere warming (*16*). In turn, an AMOC recovery associated with the warm Bølling-Allerød interstadial in the Northern Hemisphere would have led to a temporary reexpansion of Antarctic sea ice, contributing to high-latitude Southern Hemisphere cooling and stagnant atmospheric CO_2 levels during the ACR (*17*, *18*). It has been suggested, however, that invigoration of Southern Ocean overturning, sea ice retreat, and Antarctic warming at the onset of the last deglaciation may have been initiated by Southern Hemisphere processes rather than by AMOC changes induced in the North Atlantic (*4*, *8*, *19*, *20*). In particular, proxy records from the marine-influenced West Antarctic Ice Sheet Divide (WDC) ice core reveal a notable warming that began at least 2 ka before the first deglacial AMOC reduction related to Heinrich Stadial 1 (*19*). This early warming recorded in West Antarctica has been proposed to have resulted from Antarctic sea ice retreat that, in turn, may have been driven by an increasing local insolation (*19*). To reconcile the proposed driving mechanisms of sea ice changes and document their role in deglacial changes in Southern Ocean circulation, Antarctic climate, and atmospheric CO_2, it is crucial to resolve and constrain the Antarctic sea ice evolution across the last deglaciation by marine sea ice proxy evidence.

Available proxy records of Antarctic sea ice covering the last deglaciation with sufficient temporal resolution are extremely sparse.

[1]Marine Geology Section, Alfred Wegener Institute Helmholtz Centre for Polar and Marine Research, 27568 Bremerhaven, Germany. [2]Research School of Earth Sciences, Australian National University, Canberra, Australian Capital Territory 2601, Australia. [3]Climate Change Research Centre, University of New South Wales, Sydney, New South Wales 2052, Australia. [4]The Australian Centre for Excellence in Antarctic Science, University of Tasmania, Hobart, Tasmania 7001, Australia. [5]Department of Geology, Colgate University, Hamilton, NY 13346, USA. [6]Geoscience Australia, GPO Box 378, Canberra, Australian Capital Territory 2601, Australia.
*Corresponding author. Email: hsadatzki@marum.de
†Present address: MARUM-Center for Marine Environmental Sciences, University of Bremen, Bremen, Germany.
‡Deceased.

They are mostly restricted to remote Southern Ocean regions near the modern Antarctic Polar Front and mainly reflect winter sea ice conditions (*21*, *22*). Here, we present a sea ice proxy record covering the last 40 ka with a millennial-scale resolution based on molecular biomarkers from a sediment core retrieved from the modern seasonal sea ice zone off East Antarctica. Our biomarker-based sea ice record is ideally suited to trace past changes in spring/summer sea ice conditions near the Antarctic continent, where diatom assemblage data typically fail to reliably reflect glacial or deglacial sea ice conditions because of diminished productivity and opal dissolution (*23*). Combined with other proxy data and model simulation results (*18*, *24*), our sea ice record reveals unprecedented insights into East Antarctic sea ice dynamics and the underlying forcings across the last glacial–interglacial transition. Our study provides empirical evidence that supports an early initiation of deglacial Antarctic sea ice reduction driven by increasing local insolation and resolves the role of sea ice decline in facilitating Southern Ocean overturning and outgassing of CO_2 during the deglaciation, consistent with the bipolar seesaw concept.

RESULTS

Core site, chronology, and approach

Sedimentary proxy records were obtained from core IN2017_V01_C025_PC08 (in the following referred to as PC08) that was recovered from the top of a sediment ridge between two submarine canyon systems on the East Antarctic continental margin, ~200 km off the Sabrina Coast and seaward of the Moscow University Ice Shelf and the Totten Glacier (64.95°S, 120.86°E, ~2800 m water depth) (Fig. 1) (*25*). The core site is located within the seasonal sea ice zone in the southeastern Indian sector of the Southern Ocean and just north of the Dalton Polynya, where substantial amounts of sea ice are produced (*26*). Today, the retreating sea ice edge results in largely open-water conditions at core site PC08 during Austral summer and into autumn, while sea ice covers the site during the remainder of the year (Fig. 1). Core PC08 is thus ideally suited to record past changes in sea ice cover off East Antarctica, particularly with respect to shifts of the Austral summer sea ice edge and sea ice formation in the Dalton Polynya.

Down-core records of sediment color (b*), total diatom abundance, and magnetic susceptibility show a major transition in sediment composition within the upper 3 m of core PC08 investigated here (see Materials and Methods). This transition in sediment composition is characteristic of the last glacial–interglacial transition, as supported by absolute age constraints obtained for core PC08 based on 10 radiocarbon ages of acid insoluble organic matter (AIOM) (fig. S1 and table S1). An extremely low diatom abundance and increased magnetic susceptibility characterize dark gray sediments of the last glacial, indicating a strongly diminished phytoplankton production, potentially increased opal dissolution, and enhanced deposition of terrigenous detrital sediments (*27*, *28*). A rising b* reflecting yellower sediments and likely indicating an increase in opal content (*29*) is consistent with an increasing diatom abundance, which points to an enhancement of phytoplankton productivity during the deglaciation (fig. S1). An increased diatom abundance and lowered magnetic susceptibility suggest an enhanced phytoplankton production and reduced input of terrigenous material during the Holocene (*27*).

The age model of core PC08 is based on stratigraphic alignment of parallel signals in the multiproxy records of PC08 with pertinent signals in the δD record of an ice core drilled by the European Project for Ice Coring in Antarctica at Dome C (EDC) (*3*), using seven age-depth tie points (table S2). A robust alignment is enabled by variations in the b* and diatom abundance records of PC08 being remarkably consistent with the Antarctic temperature evolution across the last glacial–interglacial transition (Fig. 2, A and B). The ultrahigh-resolution b* record of PC08 even resolves short-term productivity changes that closely resemble millennial-scale Antarctic climate changes, particularly the ACR during the last deglaciation. Critically, the calibrated AIOM ^{14}C ages independently confirm the synchronicity of the increase in b* and diatom abundance and the Antarctic warming reflected by the EDC δD during the deglaciation, supporting the tuning-based age model of core PC08 (fig. S1). The chronology of PC08 places our sediment core records on the Antarctic ice core chronology AICC2012 (*30*) and reveals that the interval investigated here covers the past ~40 ka before present (BP), where the present is 1950 CE. Sedimentation rates vary between 8.7 and 9.6 cm/ka during the glacial/early deglaciation and between 3.3 and 5.7 cm/ka during the late deglaciation and Holocene, which allows resolving millennial-scale changes by our proxy records.

Enhanced sediment deposition during the glacial may largely be linked to increased deposition of terrigenous detrital material associated with advanced grounded ice on the shelf (*27*, *28*). Furthermore, the glacial diatom assemblage is marked by abundant reworked diatom taxa such as *Stephanopyxis* spp. and *Pyxilla reticulata* (fig. S2), the latter last commonly occurring in the late Oligocene (*31*). This indicates that some sediment at core site PC08 may have been advected by the westward flowing East Wind Drift current and partly lofted from turbidity currents transporting reworked, old material from the shelf downslope in the canyon systems adjacent to the core site, in addition to deposition of autochthonous hemipelagic sediment (*32*). A minor proportion of reworked old organic matter, in combination with an increased local ocean reservoir age, might also explain why the calibrated AIOM ^{14}C ages appear too old as compared with the tuning-based chronology in the glacial and early deglacial intervals (see Materials and Methods and fig. S1).

Our sea ice reconstruction is based on the sedimentary abundance of highly branched isoprenoid (HBI) lipid biomarkers produced by specific diatoms (see Materials and Methods). The di-unsaturated HBI diene has been identified in coastal Antarctic (landfast) sea ice as well as in surface sediments underlying sea ice (*33*, *34*). It is produced mainly by the sea ice diatom *Berkeleya adeliensis* (Medlin) that lives and blooms within the sea ice matrix during late spring and early summer (*34*). The HBI diene can thus be used for spring/summer sea ice reconstruction and is also referred to as the Ice Proxy for the Southern Ocean with 25 carbon atoms ($IPSO_{25}$) (*34*, *35*). On the other hand, the tri-unsaturated HBI triene (HBI-III) is produced by certain diatoms in open waters of the marginal ice zone during spring and summer (*33*, *35*). An analysis of HBI biomarkers in surface waters of the study area shows that in February to March, $IPSO_{25}$ is abundant in areas covered by summer sea ice and the Dalton Polynya (*36*). In turn, HBI-III peaks in the marginal ice zone where sea ice melts in spring/early summer and $IPSO_{25}$ is reduced (*36*). We can thus expect that paired $IPSO_{25}$ and HBI-III records of core PC08

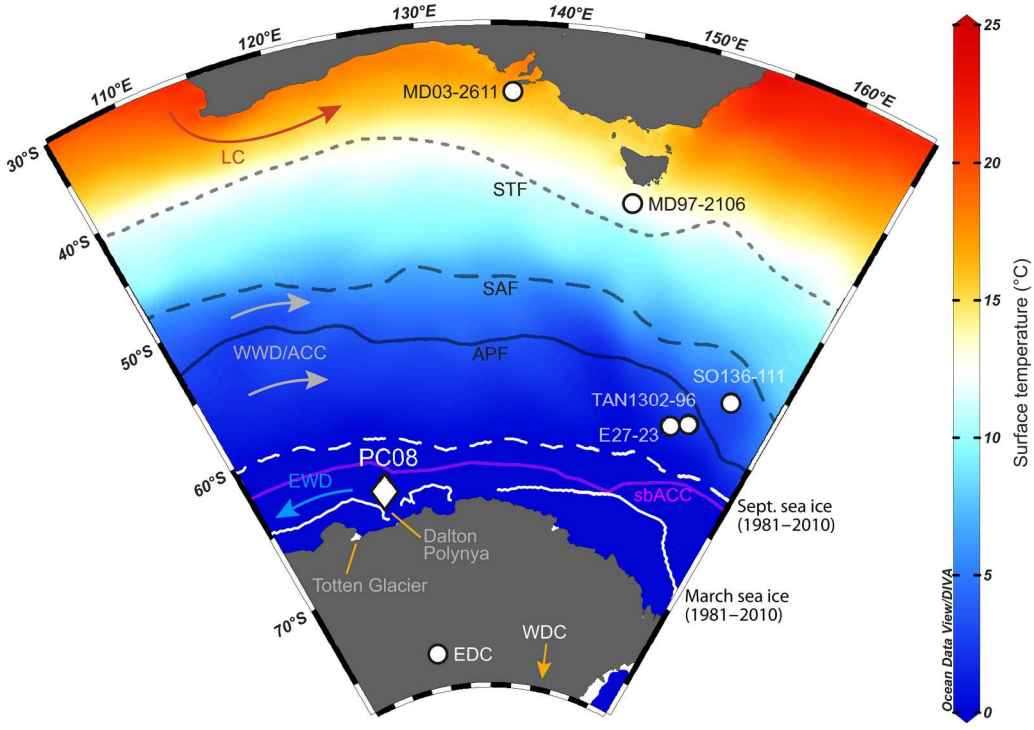

Fig. 1. Core sites and hydrography of the study area. The white diamond marks the core site investigated in this study and white circles mark other referenced core sites. The map shows annual mean sea surface temperatures based on the World Ocean Atlas 2013 database, averaged between A.D. 1955 and 2012. White lines indicate the modern sea ice extent during September (dashed) and March (solid), averaged between A.D. 1981 and 2010 (*90*). Black lines depict the main oceanic fronts (*91*), including the Antarctic Polar Front (APF), the Subantarctic Front (SAF), and the Subtropical Front (STF). Colored arrows show the main surface ocean currents, including the East Wind Drift (EWD), the West Wind Drift (WWD) or the Antarctic Circumpolar Current (ACC) with its southern boundary indicated by the pink line (sbACC), and the Leeuwin Current (LC). The map was produced with the Ocean Data View software (*92*).

reflect past changes in sea ice cover and especially shifts of the summer sea ice edge that is generally difficult to resolve by more traditional sea ice proxies such as diatom assemblage data.

We also use the phytoplankton-IPSO$_{25}$ (PIPSO$_{25}$) index and the IPSO$_{25}$/HBI-III (or diene/triene) ratio for sea ice reconstruction that are more independent of bulk accumulation rate changes than the individual biomarker concentrations (*33*, *37*) (see Materials and Methods). Analogous to the phytoplankton-IP$_{25}$ (PIP$_{25}$) index developed for the Arctic (*38*), the PIPSO$_{25}$ index allows reconstructing semiquantitative estimates of the past sea ice cover in the Southern Ocean (*37*, *39*). In principle, PIPSO$_{25}$ values can range from zero to one, indicating open-water conditions and perennial sea ice conditions, respectively, with intermediate values reflecting more or less seasonal sea ice. Moreover, our biomarker-based sea ice reconstruction is assisted by information on the relative abundance of specific diatoms that are related to sea ice or open-water conditions and compared with the simulated sea ice evolution around core site PC08 as obtained from numerical experiments with the Earth system model LOVECLIM (*18*, *24*) (see Materials and Methods).

Biomarker proxy records and sea ice reconstruction for the past 40 ka

We identified quantifiable amounts of IPSO$_{25}$ in 37 samples and HBI-III in 44 samples out of 55 samples from core PC08 with concentrations of 0.06 to 2.1 ng gSed^{-1} for IPSO$_{25}$ and 0.09 to 2.64 ng gSed^{-1} for HBI-III. IPSO$_{25}$ and HBI-III concentrations show substantial variations over the past 40 ka, with the cluster of glacial values in the IPSO$_{25}$–HBI-III cross-plot being distinctly different from the cluster of deglacial and Holocene values (Fig. 2, C and D). The resulting PIPSO$_{25}$ and IPSO$_{25}$/HBI-III records of core PC08 likewise show that IPSO$_{25}$ relative to HBI-III was increased during the glacial as compared with the deglaciation or Holocene (Fig. 2E). Although we cannot rule out a certain contribution of allochthonous biomarkers, we regard its influence on the HBI records and the glacial increase in IPSO$_{25}$, IPSO$_{25}$/HBI-III, and PIPSO$_{25}$ values in core PC08 as negligible. The glacial admixture of reworked and largely terrigenous detrital material, as reflected by the increased magnetic susceptibility, would rather lead to a dilution of individual biomarker concentrations given per gram dry bulk sediment. We thus assume that the HBI biomarker proxy records of PC08 reliably reflect the regional sea ice conditions across the last glacial–interglacial transition.

The glacial section is marked by high IPSO$_{25}$, IPSO$_{25}$/HBI-III, and PIPSO$_{25}$ values that suggest an enhanced sea ice algae production and thus increased spring/summer sea ice presence at site PC08, peaking between ~29 and ~21 ka ago, an interval comprising most of the Last Glacial Maximum (LGM) (Fig. 2). This implies a very short period of open-water conditions in late summer, allowing for some but substantially reduced phytoplankton production consistent with the total diatom abundance and b* records of core PC08. The HBI biomarker data indicate that the glacial summer

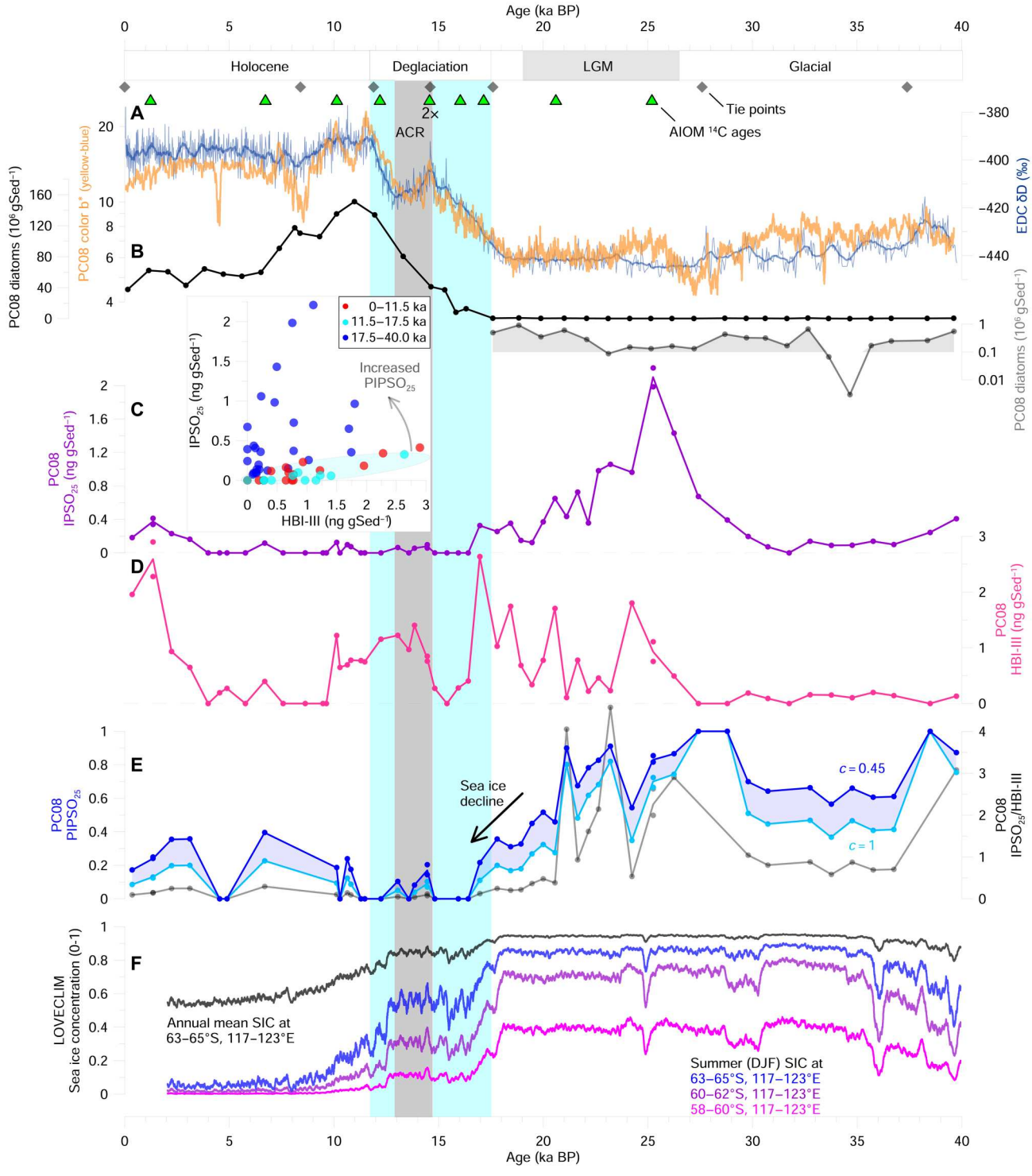

Fig. 2. Proxy records of sediment core PC08 covering the past 40 ka. (**A**) Color b* plotted as 15-point running average (orange) and δD of the EDC ice core with the thick line showing the 15-point running average (blue) (*3*, *30*). (**B**) Total diatom abundance (black), for the glacial also plotted on a logarithmic scale (gray). (**C**) $IPSO_{25}$ (purple). (**D**) HBI-III (pink). $IPSO_{25}$ and HBI-III data are also shown in a cross-plot and color-coded according to different time intervals. (**E**) $PIPSO_{25}$ (dark blue for $c = 0.45$, light blue for $c = 1$) and $IPSO_{25}$/HBI-III (gray), reflecting sea ice conditions. (**F**) Simulated annual mean sea ice concentration (black) and summer (December-January-February) sea ice concentration for core site PC08 (blue) averaged over 63°S to 65°S, 117°E to 123°E, and summer (December-January-February) sea ice concentration north of core site PC08 averaged over 60°S to 62°S, 117°E to 123°E (purple), and averaged over 58°S to 60°S, 117°E to 123°E (magenta), plotted as 101-year running averages (*18*, *24*). Gray diamonds and green triangles at the top mark positions of age-depth tie points and AIOM ^{14}C ages, respectively. Gray shading at the top indicates the LGM after Clark *et al.* (*93*). Light cyan shadings indicate phases of deglacial Antarctic warming and the gray bar marks the ACR.

sea ice edge off East Antarctica was shifted northward close to core site PC08 or even beyond during the LGM. The increased $IPSO_{25}$ and HBI-III values during the LGM could also be indicative of sea ice retention into summer and transient open-water conditions associated with the Dalton Polynya (*36*) that would have extended over site PC08. Moreover, the $PIPSO_{25}$ and $IPSO_{25}$/HBI-III records suggest rather intermediate sea ice conditions during late Marine Isotope Stage (MIS) 3 at 40 to 29 ka ago, as compared with the most extensive, yet variable spring/summer sea ice conditions during MIS 2 or the LGM (Fig. 2).

Sea ice–associated diatoms such as *Fragilariopsis curta*, *Fragilariopsis cylindrus*, and *Thalassiosira antarctica* (*40*) are largely absent and occur only sporadically in very minor proportions in the glacial section of PC08 (fig. S2). In addition, we did not identify *B. adeliensis* in any sample from core PC08, although it was found to be the main producer of $IPSO_{25}$ (*34*). This indicates that the glacial diatom assemblage in core PC08 is poorly preserved and most likely biased by selective dissolution of small and fragile sea ice diatom frustules, as typically observed in regions of summer sea ice presence and low opal export productivity (*23*). If the increased relative abundance of $IPSO_{25}$ in the glacial section of core PC08 resulted from enhanced *B. adeliensis* production, more extensive landfast ice and increased platelet ice formation might be inferred, potentially related to more advanced and melting nearby ice shelves (*34*). Nevertheless, the poorly preserved glacial diatom assemblage is consistent with a near-perennial sea ice cover at the core site as reconstructed from the HBI biomarker records, especially for the LGM.

The interval of most extensive spring/summer sea ice conditions during the LGM inferred from maximal $IPSO_{25}$ and $PIPSO_{25}$ values is followed by a decrease in $IPSO_{25}$ and a contemporaneous increase in HBI-III at ~21 to 16.5 ka ago (Fig. 2). This and the resultant stepwise decrease in $PIPSO_{25}$ values suggest a transition from near-perennial sea ice cover with enhanced summer sea ice at site PC08 to more seasonal sea ice with open-water conditions during summer. The early drop in $PIPSO_{25}$ at ~21 ka ago coincides with increases in the abundance of the seasonal sea ice diatoms *F. curta* and *F. cylindrus* and the open-water diatom *Thalassiosira lentiginosa* (fig. S2), supporting a disappearance of summer sea ice. However, a concomitant abundance increase of *T. antarctica*, which can be attributed to an early sea ice refreezing in autumn (*41*), suggests yet a relatively short open-water season. The HBI biomarker and diatom signals of initial sea ice retreat emerge ~30 cm below the onset of the major increases in total diatom abundance and b* in core PC08 (fig. S2), apparently preceding the onset of the last deglacial warming recorded by the EDC δD by several millennia according to our chronology. Another drop in $PIPSO_{25}$ at ~17.5 to 16.5 ka ago reflects the final rapid decline of spring/summer sea ice over the core site at the onset of the last deglaciation.

The deglacial section in core PC08 is characterized by low or absent $IPSO_{25}$ and variable HBI-III values, resulting in zero or low $PIPSO_{25}$ and $IPSO_{25}$/HBI-III values indicative of minimal spring/summer sea ice conditions (Fig. 2). These sections also reveal abundant diatom species characteristic of both seasonal sea ice (*F. curta* and *F. cylindrus*) and open-ocean conditions (*Fragilariopsis kerguelensis* and *T. lentiginosa*) (fig. S2). This suggests that sea ice covered core site PC08 during winter and perhaps until spring, while the HBI records and a drop in the abundance of *T. antarctica* point at an extensive open-water summer season with sea ice refreezing in late autumn during the deglaciation. Notably, zero $IPSO_{25}$ and $PIPSO_{25}$ values suggesting minimal sea ice conditions are consistent with productivity increases and coincide with deglacial Antarctic warming periods, interrupted by somewhat increased $IPSO_{25}$ and $PIPSO_{25}$ values indicating slightly enhanced spring/summer sea ice conditions during the ACR (Fig. 2).

Similar to the deglacial section, the Holocene section reveals low or absent $IPSO_{25}$, variable HBI-III values, resultant low to intermediate $PIPSO_{25}$ and $IPSO_{25}$/HBI-III values, and the presence of both seasonal sea ice diatoms (*F. curta* and *F. cylindrus*) and open-ocean diatoms (*F. kerguelensis* and *T. lentiginosa*) (Fig. 2 and fig. S2). Our Holocene HBI biomarker and diatom data reflect both sea ice algae and open-water phytoplankton production, suggesting seasonal shifts of the sea ice edge over site PC08, similar to today. Such seasonal sea ice conditions would have promoted phytoplankton productivity throughout the Holocene, in agreement with the increased total diatom abundance and b* in core PC08. Slightly increased $PIPSO_{25}$ and $IPSO_{25}$/HBI-III values during the mid- to late Holocene (apart from a drop at ~5 ka ago) and late Holocene HBI biomarker signals being similar to those just preceding the deglaciation may indicate a long-term increase in sea ice cover. This would imply a lengthening of the sea ice season and shortening of the open-water season through the Holocene, which might also be reflected by an increase in *T. antarctica* abundance and a contemporaneous reduction in total diatom abundance at 7 to 6 ka ago (fig. S2).

Proxy-based and simulated Antarctic sea ice evolution across the last glacial–interglacial transition

Our HBI biomarker records provide unprecedented insights into the spring/summer sea ice variability off East Antarctica during the past ~40 ka, suggesting a near-perennial sea ice cover at site PC08 during the last glacial and especially during the LGM, and reduced seasonal sea ice conditions during the deglaciation and the Holocene. The overall glacial–interglacial sea ice changes as well as trends of an increasing sea ice cover from MIS 3 to the LGM and through the Holocene, as shown by our $PIPSO_{25}$ record of PC08, generally agree with orbital-scale changes and trends observed in several diatom-based (winter) sea ice records from various Southern Ocean regions (*22*, *42*). Diatom-based sea ice records of sediment cores E27-23 (*43*), TAN1302-96 (*44*), and SO136-111 (*45*) from the southwest Pacific sector of the Southern Ocean (Fig. 1), for example, indicate enhanced winter sea ice conditions near the modern Antarctic Polar Front during the last glacial, and much reduced, only occasional winter sea ice during the deglaciation and the Holocene (fig. S3). The diatom records of the two distal core sites TAN1302-96 and SO136-111 also suggest that winter sea ice retreat in the Pacific sector started at ~20 to 21 ka ago (*22*), consistent with the early spring/summer sea ice retreat reflected by the $PIPSO_{25}$ record of PC08 (fig. S3). Other Southern Ocean regions showed later winter sea ice reductions that rather paralleled the major deglacial Antarctic warming (*22*, *42*).

Our results support an increased LGM summer sea ice extent that was also derived from circum-Antarctic micropaleontological evidence, though with considerably less confidence than a greater LGM winter sea ice extent (*46*). However, our sea ice record suggests the greatest summer sea ice extent at ~29 to 21 ka ago, which not only partly overlaps but also differs from the LGM time slice definition (23 to 19 ka ago) used for the reconstructions of the "Multiproxy Approach for the Reconstruction of the Glacial

Ocean Surface" project (*46*). Nevertheless, the maximal summer sea ice cover at ~29 to 21 ka ago in our record from the southeastern Indian sector agrees with a period of maximal summer sea ice extent at either ~31 to 23.5 ka ago (*47*) or ~30 to 22 ka ago (*48*) reconstructed on the basis of diatom records from the Scotia Sea in the southwestern Atlantic sector of the Southern Ocean. Moreover, the diatom records from the Scotia Sea suggest that summer sea ice retreat in the southwestern Atlantic sector initiated as early as ~23.5 to 22 ka ago and was followed by winter sea ice retreat (*47*, *48*). This is fairly consistent with the initial spring/summer sea ice retreat at ~21 ka ago in our $PIPSO_{25}$ record of PC08, despite potential age model offsets between the different cores. The marine proxy evidence thus indicates that the glacial Antarctic summer sea ice cover in different Southern Ocean sectors started to decline several millennia before the onset of the major deglacial Antarctic warming and atmospheric CO_2 rise at ~17.5 ka ago (*49*).

Furthermore, the sea ice variability in the $PIPSO_{25}$ record of PC08 agrees in parts with the simulated sea ice concentration evolution obtained from transient numerical experiments performed with the Earth system model LOVECLIM (*18*, *24*). Around site PC08, the transient simulation displays an increase in summer sea ice concentration from 50% at 40 ka ago to maximal coverage of 90% at 32 ka ago, followed by relatively stable glacial sea ice concentration until ~18 ka ago, with only a minor ~5% decrease from 32 to 18 ka ago (Fig. 2F). The sea ice concentration decreases during the deglaciation to reach summer ice-free conditions at 8 ka ago. Superimposed on these long-term sea ice variations related to changes in orbital parameters, ice sheet orography and surface albedo, and atmospheric greenhouse gases, the simulation reveals abrupt sea ice reductions associated with reductions of the AMOC induced by freshwater forcing to the North Atlantic (fig. S4). The reduced northward oceanic heat transport in the Atlantic resulting from the AMOC weakening leads to a warming of the South Atlantic. This anomalous heat is advected to the Southern Ocean through the Antarctic Circumpolar Current, thus leading to Antarctic sea ice retreat. The simulated sea ice reduction is larger for Heinrich Stadial 1 (here simulated at 18 to 15 ka ago) than for Heinrich Stadials 2 or 3 (here simulated at 25.9 to 24.2 ka ago and 31.3 to 28.7 ka ago, respectively), because the AMOC reduction lasts longer and because of the concurrent atmospheric CO_2 increase (*1*, *2*).

The transient simulation reveals a fairly rapid sea ice decline during early Heinrich Stadial 1, a sea ice readvance (from 45 to 60%) during the ACR, and another rapid sea ice decline at the onset of the Younger Dryas, which resembles well the sea ice variations reflected by the $PIPSO_{25}$ record of PC08 (Fig. 2). The simulated summer sea ice concentrations at 60°S to 62°S or 58°S to 60°S reveal that most of the glacial–interglacial sea ice reduction happened by ~16 ka ago, more consistent with the $PIPSO_{25}$ record than the simulated sea ice cover for site PC08 (Fig. 2F and fig. S4). This indicates that the simulated LGM summer sea ice cover might be overestimated somewhat, although it is close to proxy estimates and the Paleoclimate Modeling Intercomparison Project 4 (PMIP4) multimodel mean (*50*). In contrast with the proxy records of PC08, however, the model simulation reveals neither a substantial sea ice reduction between 21 and 18 ka ago nor a trend of an increasing sea ice cover through the Holocene.

Last, the sea ice variability reflected by the $PIPSO_{25}$ record of PC08 for the past ~40 ka shows some agreements and some disagreements with sea salt sodium (ssNa) records of the EDC (*51*, *52*) and WDC ice cores (*19*) that are affected not only by changes in sea ice production/extent but also by atmospheric circulation and aerosol transport pathway. The ssNa records of both Antarctic ice cores show an increased glacial sea ice cover as well as trends of increasing sea ice during the glacial and the Holocene, generally consistent with our $PIPSO_{25}$ record (Fig. 3). However, the major sea ice reduction in the EDC ssNa record occurs during the deglaciation and thus much later than in either our $PIPSO_{25}$ record or the WDC ssNa record. The deglacial sea ice retreat in the EDC ssNa record rather resembles the sea ice evolution in the transient simulation (fig. S4). The high-altitude EDC ssNa record may thus reflect large-scale changes in winter sea ice conditions in the Indian sector (*51*, *52*) but not necessarily summer sea ice changes proximal to the Antarctic continent that are recorded by the $PIPSO_{25}$ of PC08. On the other hand, the nature and timing of sea ice variations reflected by the ssNa record of the marine-influenced WDC ice core are very consistent with those reflected by the $PIPSO_{25}$ record of PC08 (Fig. 3). This includes maximal sea ice conditions during MIS 2, an early sea ice retreat preceding minimal sea ice conditions during the deglaciation, and sea ice readvance during the ACR. Hence, Southern Ocean regions off East Antarctica and West Antarctica were apparently marked by similar sea ice dynamics across the last glacial–interglacial transition, pointing at common forcings.

DISCUSSION

Our results reveal a near-perennial sea ice cover at core site PC08 during the last glacial and especially at ~29 to 21 ka ago, followed by sea ice reduction between ~21 and ~16.5 ka ago, and reduced spring/summer sea ice conditions during the deglaciation and the Holocene. The spring/summer sea ice variability reflected by the $PIPSO_{25}$ record of PC08 is consistent with latitudinal shifts of the Southern Ocean fronts as reconstructed by changes in the relative abundance of subpolar planktic foraminifera in core MD03-2611 from the continental margin south of Australia (Fig. 1) (*53*, *54*). This record of core MD03-2611 indicates a northward shift of the Subantarctic Front and the Antarctic Polar Front contemporaneously with enhanced sea ice cover off East Antarctica during the last glacial, particularly during MIS 2 and, to a lesser extent, during late MIS 3 (Fig. 3). A piecewise linear interpolation of the $PIPSO_{25}$ record of PC08 shows that 50% and thus a substantial portion of the glacial–interglacial sea ice reduction had happened by ~19.5 ka ago (pink dashed line in Fig. 3), which coincides exactly with a southward shift of the Subantarctic Front and the Antarctic Polar Front as derived from a decline in subpolar planktic foraminifera abundance in core MD03-2611. This substantial sea ice reduction off East Antarctica and the associated southward shift of the Southern Ocean fronts is also concomitant with the onset of sea ice reduction and resultant atmospheric warming off West Antarctica as recorded by the ssNa and $\delta^{18}O$ records of the WDC ice core (*19*). Our $PIPSO_{25}$ record of core PC08, the subpolar foraminifera abundance record of well-dated core MD03-2611, and the well-constrained WDC ice core records thus provide independent lines of evidence supporting that early sea ice and surface ocean changes in the Southern Ocean initiated as early as ~19.5 ka ago (with signs of summer sea ice retreat in our reconstruction as early as ~21 ka ago) and thus (at least) about 2 ka before major deglacial changes in global ocean circulation, climate, and atmospheric CO_2 (*49*).

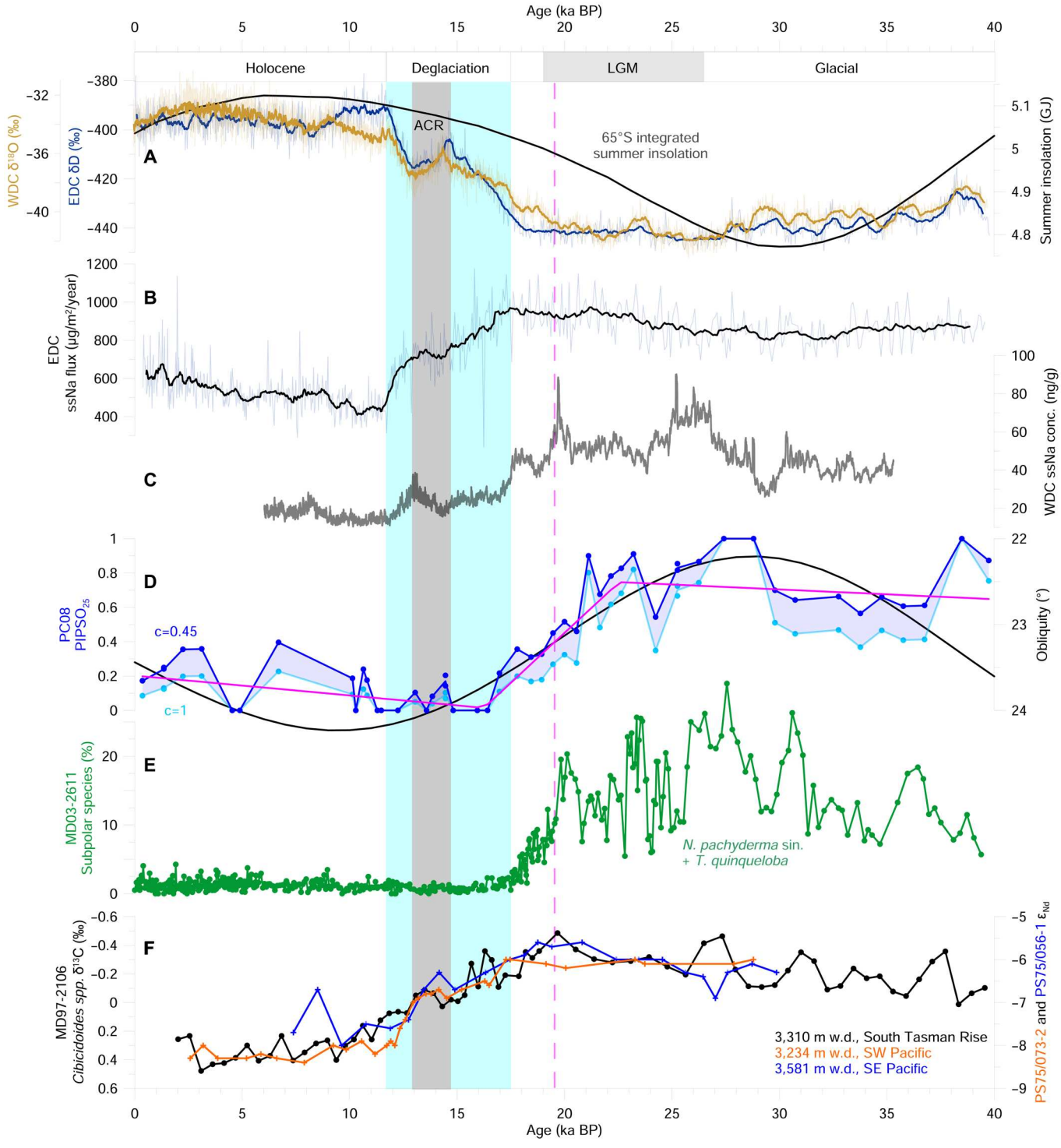

Fig. 3. Antarctic sea ice records and other environmental proxy records covering the last glacial–interglacial transition. (**A**) δD of the EDC ice core (blue) (*3*, *30*) and $\delta^{18}O$ of the WDC ice core (orange) (*19*, *94*, *95*) with the thick lines showing the 15-point running averages, and integrated summer insolation at 65°S for a diurnal average insolation threshold of 275 W/m^2 (gray) (*57*, *96*). (**B**) ssNa flux of the EDC ice core with the thick line showing the 15-point running average (*52*). (**C**) ssNa concentration of the WDC ice core with the thick line showing the 25-point running average (*19*, *94*, *95*). (**D**) $PIPSO_{25}$ of core PC08 (dark blue for $c = 0.45$, light blue for $c = 1$) with its combined piecewise linear interpolation (pink) and obliquity (gray) (*97*). (**E**) Subpolar planktic foraminifera abundance of core MD03-2611 (*53*) on the latest chronology according to De Deckker *et al.* (*54*). (**F**) Benthic foraminiferal $\delta^{13}C$ of core MD97-2106 (*60*) on the latest chronology according to Moy *et al.* (black) (*98*) and ε_{Nd} of fish teeth/debris and manganese/iron coatings in foraminifera of cores PS75/073-2 (orange) and PS75/056-1 (blue) (*4*). The vertical pink dashed line marks the midpoint of the linearly interpolated $PIPSO_{25}$ decrease, at which 50% and thus a substantial portion of the glacial-interglacial sea ice reduction had happened. Gray shading at the top indicates the LGM after Clark *et al.* (*93*). Light cyan shadings indicate phases of deglacial Antarctic warming and the gray bar marks the ACR.

It has been suggested that local orbital forcing contributed to early glacial–interglacial changes in Antarctic sea ice and high-latitude Southern Hemisphere climate (*19*, *55*, *56*). Our $PIPSO_{25}$ record shows that the Antarctic sea ice cover varied largely in harmony with obliquity changes over the last 40 ka (Fig. 3D). Critically, the obliquity is the primary control of the summer insolation integrated over the duration of the summer (*57*). The local integrated summer insolation at 65°S, where summer is defined as days with the diurnal average insolation exceeding a threshold of 275 W/m^2, gradually increased from the last glacial to the Holocene and had reached ~50% of the glacial–interglacial amplitude at 19.5 ka ago (Fig. 3A). This early increase in local integrated summer insolation at 65°S, which is independent of the longitude, may have thus provided enough energy to initiate melting of the near-perennial sea ice cover in late glacial summer at site PC08 off East Antarctica and induce concomitant early sea ice retreat off West Antarctica as observed in the WDC ssNa record (*19*).

The transient simulation performed with LOVECLIM supports an obliquity-related forcing of the summer sea ice variability over the past 40 ka, albeit with a different sensitivity than illustrated by the $PIPSO_{25}$ record of PC08 (Fig. 2, E and F). The simulated summer sea ice cover around site PC08 is not sufficiently sensitive to insolation changes to show a notable sea ice retreat in response to an obliquity increase at ~21 to 18 ka ago or sea ice increase in response to an obliquity decrease during the late Holocene. Nevertheless, the glacial–interglacial sea ice reduction in the model simulation can be linked to a combination of an increasing integrated summer insolation over the Southern Ocean and ocean-atmosphere interhemispheric teleconnections associated with an AMOC reduction. The experiment was designed such that the AMOC reductions in the model simulation occur at a similar time as those suggested by $^{231}Pa/^{230}Th$ proxy evidence for Heinrich Stadial 1 and the Younger Dryas (*14*) (fig. S4E). It should be noted that there is some evidence of an early freshwater release to the North Atlantic from melting of the Eurasian ice sheet around ~20 ka ago (*58*, *59*), which potentially could have perturbed the AMOC but was not taken into account here. Thus, we cannot exclude an influence of an AMOC reduction on the early initiation of Antarctic sea ice retreat observed in the proxy records but regard that influence as uncertain compared to that of an increasing integrated summer insolation over the high-latitude Southern Ocean.

The poleward shift of the spring/summer sea ice edge and oceanic fronts off East Antarctica across the last glacial–interglacial transition was accompanied by a regime shift from an increased stratification between abyssal and deep waters to an enhanced mixing of the water column in the Southern Ocean. It has been suggested that in the Southern Ocean, the upper circulation cell (bearing North Atlantic Component Water) and the lower circulation cell (bearing Southern Component Water) were decoupled during the last glacial (*4*, *8*–*10*). In turn, increased mixing between the circulation cells led to enhanced incorporation of North Atlantic Component Water into Southern Ocean deep waters during the Holocene (*4*, *8*–*10*). This is reflected by the increasing benthic foraminiferal $\delta^{13}C$ in core MD97-2106 from south of Tasmania (*60*) and decreasing ε_{Nd} of fish teeth/debris and manganese/iron coatings in foraminifera in cores PS75/073-2 and PS75/056-1 from the South Pacific (*4*) across the last glacial–interglacial transition (Fig. 3F). Our results are consistent with the notion that a reduction of the (summer) sea ice cover changed the sea-air buoyancy flux and geometry of the density surfaces in the Southern Ocean, thereby contributing to a deepening of the boundary between abyssal and deep waters, increasing the diapycnal mixing between the two circulation cells through the interaction of the abyssal current with the bottom topography (*9*, *10*). Our $PIPSO_{25}$ record could also be consistent with a reduction in sea ice formation and associated brine rejection across the last glacial–interglacial transition, which might have decreased the volume and/or density of Antarctic Bottom Water, thereby reducing the deep stratification (*10*). We speculate that the early sea ice reduction before the onset of the deglaciation, as recorded by the $PIPSO_{25}$ record of PC08, might have been coupled with an initial decrease in the stratification between abyssal and deep waters. This seems to be supported by deep-sea coral ε_{Nd} records from the Drake Passage reflecting enhanced mixing between the lower and upper circulation cells at ~20 to 18 ka ago (*8*), and with $^{231}Pa/^{230}Th$ records from the deep southwestern Pacific indicating an increase in South Pacific overturning initiating as early as 20 ka ago (*20*). Nevertheless, our results suggest that the major breakup of the glacial deep stratification in the Southern Ocean coincided with minimal Antarctic summer (and winter) sea ice conditions that would have facilitated effective deep winter convection and large-scale turbulent mixing during the deglaciation, where temporary sea ice reexpansion contributed to a halt in stratification breakup during the ACR (Fig. 3) (*4*, *8*).

At the onset of the deglaciation, the rapid sea ice decline reflected by the $PIPSO_{25}$ record of PC08 is concomitant with (or just preceded by) a surface ocean warming south of Australia recorded in core MD03-2611 (*53*, *54*) and the major AMOC reduction related to Heinrich Stadial 1 that is evidenced by the $^{231}Pa/^{230}Th$ record from the North Atlantic (*14*) (Fig. 4). Similarly, following the minor sea ice readvance and reinvigorated AMOC during the ACR, sea ice reduction off East Antarctica occurred again contemporaneously with surface warming south of Australia and the AMOC reduction during the Younger Dryas. The warming south of Australia suggests a southward shift of the Subtropical Front and increased advection of warm subtropical surface waters via the Leeuwin Current, driven by a southward shift of the Southern Hemisphere westerly winds (Fig. 1) (*53*, *54*). This supports the idea that an AMOC reduction and Northern Hemisphere cooling were accompanied by interhemispheric teleconnections that led to a poleward shift of the Southern Hemisphere westerly winds and Southern Ocean fronts. These teleconnections and ocean-atmosphere changes in the Southern Ocean, despite its thermal inertia, were apparently also accompanied by a fairly rapid reduction of the (already declining) sea ice cover off East Antarctica during early Heinrich Stadial 1 and at the onset of the Younger Dryas, although changes in the Subantarctic were much more rapid (*12*). A reinvigorated AMOC and associated enhanced meridional ocean heat transport may have resulted in surface-ocean cooling and sea ice readvance at southern high latitudes during the ACR (*17*, *18*), consistent with the concept of the bipolar seesaw. Similar to the millennial-scale dynamics during the deglaciation, the temporary Antarctic sea ice reduction, southward shift of Southern Ocean fronts, and Antarctic warming observed at ~24 ka ago in the proxy records might be attributed to the AMOC weakening during Heinrich Stadial 2, which is in agreement with the transient LOVECLIM model simulation and also corroborates the somewhat

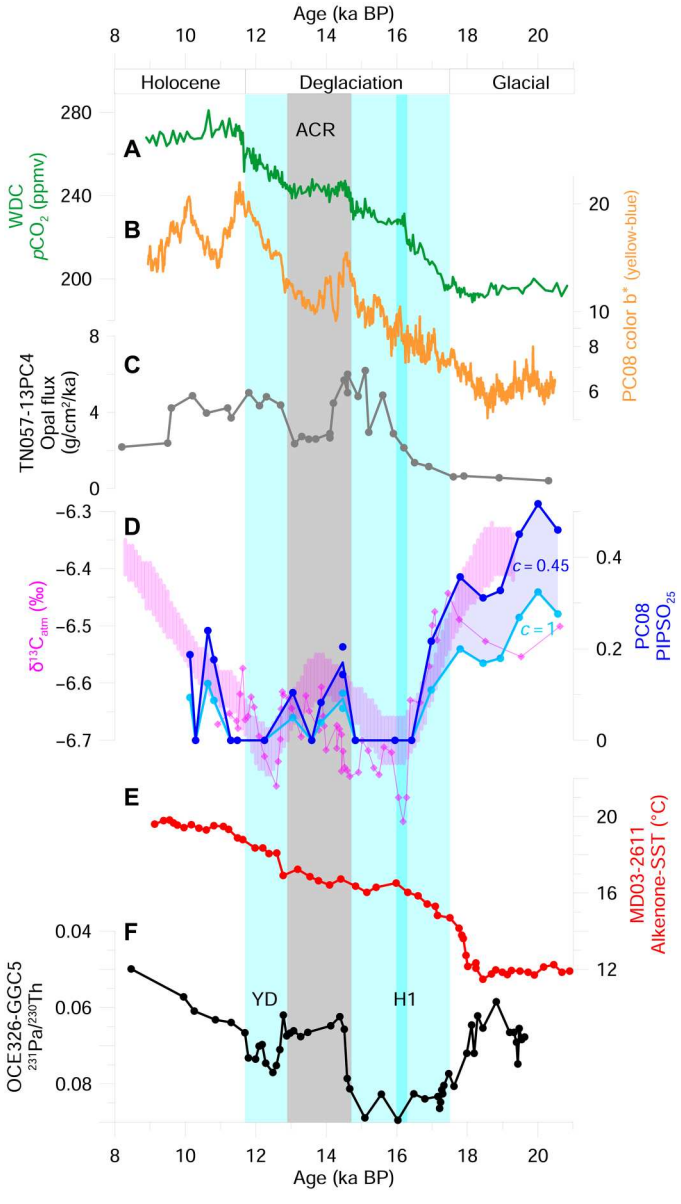

Fig. 4. Deglacial records of Antarctic sea ice, ocean circulation, and atmospheric CO_2. (**A**) Atmospheric pCO_2 of the WDC ice core (green) (*70*). (**B**) Color b* plotted as 15-point running average (orange). (**C**) Opal flux of core TN057-13PC4 (*6*). (**D**) $PIPSO_{25}$ of core PC08 (dark blue for $c = 0.45$, light blue for $c = 1$) and the $\delta^{13}C_{atm}$ of atmospheric pCO_2 from Taylor Glacier (*69*) (magenta diamonds) and from three Antarctic ice cores (*68*, *99*) (magenta SE bars of a Monte Carlo average). (**E**) Alkenone-based sea surface temperature (SST) record of core MD03-2611 (*54*). (**F**) Sedimentary $^{231}Pa/^{230}Th$ record of core OCE326-GGC5 (*14*). Light cyan shadings indicate phases of deglacial Antarctic warming, concurrent with major reductions in the AMOC associated with Heinrich Stadial 1 (H1) and the Younger Dryas (YD), and the gray bar marks the ACR. The darker cyan shading marks centennial-scale Southern Ocean overturning/outgassing and the associated rapid atmospheric CO_2 rise at ~16.3 ka ago.

uncertain chronology of the glacial section in core PC08 (Fig. 3 and fig. S4).

It has been suggested that the poleward shift and/or strengthening of the Southern Hemisphere westerly winds associated with AMOC reductions induced enhanced upwelling in the Southern Ocean and CO_2 outgassing to the atmosphere during the last deglaciation (*6*, *7*, *16*, *61*, *62*). Enhanced upwelling during Heinrich Stadial 1 and the Younger Dryas has been inferred, for example, from peaks in the opal burial rates observed in the Antarctic zone south of the modern Polar Front, as upwelled nutrient-rich deep waters would have stimulated the phytoplankton and export production (*6*). The deglacial changes in the opal flux recorded in core TN057-13PC4 from the Atlantic Southern Ocean are in general agreement with the b* record of PC08 (Fig. 4, B and C). The increasing deglacial productivity recorded in core PC08 might have resulted from reduced seasonal sea ice conditions and enhanced upwelling through Ekman divergence at the southern boundary of the Antarctic Circumpolar Current, which probably also shifted poleward during the deglaciation close to its modern position near the core site (Fig. 1). Our age model approach and the presumed remarkable correspondence between productivity increases and peaks reflected by the b* record of PC08 and deglacial atmospheric CO_2 rises on millennial and centennial time scales (Fig. 4, A and B) are consistent with the proposed close link between productivity/upwelling in the Antarctic zone and atmospheric CO_2 (*63*). Apparently, the initial sea ice retreat starting at ~21 ka ago was not accompanied by a noticeable productivity increase, possibly due to yet limited upward mixing of nutrient-rich subsurface waters under an extensive surface stratification resulting from seasonal sea ice melting until the onset of the deglaciation. The increased deglacial phytoplankton production in the Antarctic zone must then have been accompanied by an inefficient nutrient utilization to produce a leak in the biological pump and allow outgassing of CO_2 to the atmosphere (*64*, *65*).

Ventilation age and pH reconstructions for Southern Ocean deep waters indeed document deglacial periods of carbon release associated with millennial- and centennial-scale rises in atmospheric CO_2, after very old and carbon-enriched waters had accumulated in the stratified deep ocean during the LGM (*5*, *65*–*67*). Outgassing of CO_2 from upwelled old and carbon-enriched waters in the Southern Ocean may also be reflected by pronounced drops in atmospheric $\delta^{13}C$ observed in ice core records contemporaneously with atmospheric CO_2 rises during Heinrich Stadial 1 and the Younger Dryas (*62*, *68*, *69*). A close correspondence of variations in atmospheric $\delta^{13}C$ and $PIPSO_{25}$ of core PC08 suggests a tight coupling between increased Southern Ocean upwelling/outgassing and Antarctic sea ice reduction during the deglaciation (Fig. 4D). Moreover, century-scale abrupt drops in atmospheric $\delta^{13}C$ and increases in Antarctic zone productivity during mid-Heinrich Stadial 1 and at the onset of the Younger Dryas immediately followed rapid deglacial sea ice reductions observed in the $PIPSO_{25}$ record of PC08. This illustrates that Antarctic sea ice decline might have acted as a tipping element that contributed to an abrupt intensification of Southern Ocean upwelling/outgassing and the associated centennial-scale rise in atmospheric CO_2 at ~16.3 ka ago and, though more gradual, CO_2 rise at ~12.9 ka ago (*6*, *69*, *70*). Our results thus support hypotheses that relate the enhanced outgassing of CO_2 from the Southern Ocean and deglacial atmospheric CO_2 rises to mechanisms including a reduction of the Antarctic sea ice cover,

for example, by increasing the time and space for sea-air gas exchange (*11*) and interacting with Southern Ocean circulation (*9*, *10*).

In conclusion, our study provides unprecedented proxy evidence that resolves an increased spring/summer sea ice cover off East Antarctica during the last glacial, particularly during the LGM or MIS 2, which likely contributed to an enhanced deep stratification and reduced outgassing of CO_2 in the Southern Ocean. In line with evidence from other Southern Ocean sectors (*19*, *47*–*49*), our results reveal an early Antarctic sea ice decline at the last glacial–interglacial climate transition, probably initiated by an increasing local integrated summer insolation. We surmise that the early Antarctic sea ice decline might have played a leading role in the initiation of deep Southern Ocean stratification breakup, while a presumably associated early climate warming, as recorded by the WDC ice core, yet needs to be resolved for coastal East Antarctica. This early Antarctic sea ice retreat apparently preceded the deglacial atmospheric CO_2 rise and we suggest that surface stratification resulting from sea ice melting during summer possibly acted as a mechanism to suppress upward mixing of deeper waters to the surface and delay outgassing of CO_2 from the Southern Ocean (*49*). Subsequent deglacial sea ice reductions were tightly coupled with enhanced Southern Ocean upwelling and outgassing of CO_2, associated with AMOC weakening, thus facilitating atmospheric CO_2 rise and contributing to major Antarctic warming. Our findings underpin the instrumental role of changes in the Antarctic sea ice cover in contributing to and possibly instigating changes in Southern Ocean overturning, atmospheric CO_2, and Antarctic climate at the last glacial–interglacial transition.

MATERIALS AND METHODS

Sediment material and analyses of physical properties

Piston core PC08 (IN2017_V01_C025_PC08) investigated in this study was recovered from the Sabrina coast slope northeast of the Totten Glacier off East Antarctica (64.95°S, 120.86°E, ~2800 m water depth) during RV *Investigator* expedition IN2017_V01 in 2017 (Fig. 1) (*25*). Core PC08 is 12.1 m long, but in this study, we focused on the uppermost ~300 cm. Sediments consist of greenish gray, silty clay with some ice rafted debris in glacial sections and light gray and brown, diatom-rich silt in interglacial sections. The sediment color b* was analyzed at the Research School of Earth Science, Australian National University, using an Avaatech core-scanner equipped with a digital Color Line camera. After smoothing of the sediment surface, analyses were performed on the archive half of core PC08, and color parameters were obtained at a spacing of 70 μm. The magnetic susceptibility was analyzed at Geoscience Australia, using a handheld Magnetic Susceptibility meter. Analyses were performed on the archive half of core PC08 at a spacing of 1 cm.

Diatom analysis

Sediment subsamples for diatom analysis were taken from core PC08 at a spacing of 5 to 10 cm and analyzed at the Department of Geology, Colgate University. Quantitative diatom slides were prepared according to the settling technique of Warnock and Scherer (*71*) and inspected under Olympus CX31 and BX60 microscopes, using a 100× oil immersion objective for a total magnification of ×1000. For each slide, a minimum of 400 valves was counted for diatom-rich samples, or 10 transects were counted for diatom-poor samples, only considering valves that were >50% intact. Diatom counts are given per gram dry weight of the sediment subsamples analyzed. Where possible, diatoms were identified to species level following Armand *et al.* (*40*), Cefarelli *et al.* (*72*), and Crosta *et al.* (*73*).

Biomarker analysis

Sediment subsamples for molecular biomarker analysis were taken from core PC08 at a spacing of 1 to 10 cm and analyzed for HBI biomarkers (indicative of sea ice and open-ocean diatoms) at the Research School of Earth Sciences, Australian National University, following standardized methods for extraction and analysis of HBIs (*74*, *75*). Biomarkers were extracted from ~5 g of freeze-dried and homogenized sediment using ultrasonication with dichloromethane:methanol (2:1, v/v) as solvent. Before extraction, the internal standard 9-octyl-8-heptadecene (9-OHD; 10 μl; 2.5 μg ml^{-1}) was added to each sample to enable quantification of HBI biomarkers. After centrifugation (2500 rpm, 90 s), the supernatant was decanted into a clean glass vial, and the extraction procedure was repeated twice more. After removal of the solvent from the combined total organic extract under a gentle N_2 stream, the dried extracts were resuspended in *n*-hexane (~0.5 ml). Extracts were then separated into a hydrocarbon fraction containing HBIs and a polar fraction through open-column chromatography (SiO_2) using 5 ml of *n*-hexane and 5 ml of dichloromethane:methanol (1:1, v/v), respectively.

HBIs in the hydrocarbon fraction were analyzed by gas chromatography/mass spectrometry using an Agilent 6890 gas chromatograph (GC) coupled to a Micromass AutoSpec Premier mass spectrometer (MS; Waters Corporation, Milford, MA, USA) in selected ion recording mode. The GC was equipped with a 60-m DB-5 capillary column (0.25-mm inner diameter, 0.25-μm film thickness; Agilent J&W Scientific, Agilent Technologies, Santa Clara, CA, USA), and helium was used as the carrier gas at a constant flow of 1 ml min^{-1}. Samples were injected in splitless mode into a Gerstel programmable temperature vaporizer (PTV) injector at 60°C (held for 0.1 min) and heated at 260°C min^{-1} to 300°C. The MS source was operated at 260°C in electron ionization (EI) mode at 70-eV ionization energy and 8000 V acceleration voltage. All samples were injected in *n*-hexane to avoid deterioration of chromatographic signals by $FeCl_2$ buildup in the MS ion source through the use of halogenated solvents (*76*). The GC oven was programmed from 60° to 315°C at 10°C min^{-1} and held at 315°C for 10 min, with a total run time of 43 min.

Identification of the HBI diene ($IPSO_{25}$; indicative of sea ice diatoms) and HBI triene (HBI-III; indicative of open-ocean diatoms) was based on comparison of GC retention times with those of reference compounds and published mass spectra (*77*). $IPSO_{25}$ and HBI-III were quantified using their molecular ion mass-charge ratio (*m*/*z*) 348.3 and *m*/*z* 346.3, respectively, in relation to the abundant fragment ion *m*/*z* 350.3 of the internal standard 9-OHD. To account for differential mass spectral responses between a particular HBI and the internal standard, we used a GC-MS response factor (RF) for estimating HBI concentrations. The RF was obtained by analyzing reference sediment with known $IPSO_{25}$ and HBI-III concentrations along with each sequence of samples analyzed over a period of 4 months (RF averaged 5.52 for $IPSO_{25}$ and 10.32 for HBI-III). Replicate analyses of PC08 samples at 6.5, 74.5, and 171.5 cm core depth indicate the

reproducibility of our HBI measurements, showing averages and SDs of 0.38 ± 0.05 ng g^{-1}, 0.08 ± 0.03 ng g^{-1}, and 2.10 ± 0.16 ng g^{-1} for $IPSO_{25}$, and 2.59 ± 0.44 ng g^{-1}, 0.81 ± 0.06 ng g^{-1}, and 0.93 ± 0.25 ng g^{-1} for HBI-III, respectively.

To generate semiquantitative estimates of the past sea ice cover, we calculated the phytoplankton-$IPSO_{25}$ index ($PIPSO_{25}$) established for the Southern Ocean (*37*, *39*), analogous to the phytoplankton-IP_{25} index developed for the Arctic (*38*):

$$PIPSO_{25} = [IPSO_{25}]/\{[IPSO_{25}] + ([\text{phytoplankton marker}] \times c)\}$$

As a phytoplankton marker, we used HBI-III. The balance factor c corresponds to the ratio of the average $IPSO_{25}$ and HBI-III concentrations for all PC08 samples investigated in this study ($c = 0.45$). In addition, we also show $PIPSO_{25}$ values calculated for $c = 1$. The replicates at 6.5, 74.5, and 171.5 cm in PC08 suggest an SD of ≤0.04 for $PIPSO_{25}$ values.

Radiocarbon dating of AIOM

Radiocarbon (^{14}C) dating of AIOM of marine and potentially terrestrial origin was performed at the Research School of Earth Sciences, Australian National University, using 10 sediment samples from certain stratigraphic levels within the upper 171.5 cm of core PC08. For each sample, ~250 mg of freeze-dried and homogenized bulk sediment was repeatedly acidified (0.1 M HCl), rinsed three times with ultrapure 18-megohm water, and centrifuged to remove acid-soluble organic matter and inorganic carbon. The remaining AIOM was freeze-dried and subsequently combusted (900°C, 6 hours) after adding CuO and Ag to each sample to oxidize the organic matter to CO_2. The CO_2 was converted to graphite using H_2 and iron powder. The graphite samples were then measured on the single-stage accelerator MS at the Australian National University. Samples were normalized using oxalic acid I, background subtracted with ^{14}C-free material (coal). Results are presented as suggested by Stuiver and Polach (*78*). A replicate AIOM ^{14}C analysis of the sediment sample from 74.5-cm core depth reveals a minor age difference of 220 years and thus good reproducibility of mid-deglacial AIOM ^{14}C ages.

Conventional AIOM ^{14}C ages were calibrated to calendar ages using Calib 8.20 (*79*), the MARINE20 calibration curve (*80*), and two different additional reservoir age correction (ΔR) scenarios to consider the effect of variable sea ice conditions in polar regions (table S1) (*81*). A low ^{14}C-depletion scenario accounts for minimal regional ^{14}C depletion as might be expected for Holocene times, for which we used a ΔR^{Hol} of 440 ± 80 years. This ΔR^{Hol} estimate is based on the rounded difference between an average ^{14}C age of 1048 ± 52 years obtained from three mollusk shells from Kerguelen Islands in the southern South Indian for the period between 1909 and 1931 (*82*), and the mean of nonpolar global average marine ^{14}C age from the MARINE20 calibration curve for the period from 1910 to 1930 (605 ± 63 years). A high ^{14}C-depletion scenario accounts for an additional, local ^{14}C depletion related to an increased sea ice cover as might be expected for cold stages, for which we used a ΔR^{CS} of 1600 ± 80 years. This ΔR^{CS} estimate is obtained by adding 1160 years to the ΔR^{Hol} estimate following recommendations for a latitude-dependent reservoir age correction based on a model simulation of an extreme glacial (CS) scenario (*81*).

Chronology

Down-core records of sediment color (b*), total diatom abundance, and magnetic susceptibility show a major transition in sediment composition within the upper 3 m of core PC08 investigated here. Previous studies investigating other sediment cores from the Sabrina coast slope off East Antarctica have shown that this major transition in sediment composition reflects an increase in phytoplankton productivity and decrease in terrigenous sediment input, which is characteristic of the last glacial–interglacial transition (*27*, *28*). This is independently supported by absolute age constraints obtained for core PC08 based on 10 calibrated AIOM ^{14}C ages (table S1). The AIOM ^{14}C ages suggest that the bulk organic matter in the upper 172 cm of core PC08 is of Holocene, deglacial, and late glacial ages, considering both a Holocene and a glacial reservoir age correction scenario (table S1). However, potentially underestimated local marine reservoir ages and a potential contribution of some reworked old organic matter would result in an overestimation of the calibrated ages, thus hampering a meaningful calibration of the AIOM ^{14}C ages (*83*). These processes might also explain the occurrence of two age reversals observed at 55.5 and 126.5 cm core depth. We thus refrain from basing the chronology of core PC08 entirely on the AIOM ^{14}C ages, yet they provide independent maximum age constraints.

Instead, we used the continuous and high-resolution records of sediment color b*, total diatom abundance, and magnetic susceptibility for stratigraphic alignment and the chronology of core PC08. The b* was shown to reflect the biogenic opal content in sediments from the Scotia Sea (*29*). This is consistent with concurrent variations of the b* and total diatom abundance in core PC08 that most likely both reflect biogenic opal and, by extension, local phytoplankton productivity. It has been shown that the productivity in the Antarctic zone was closely coupled with Antarctic and global climate changes during the Late Pleistocene glacial–interglacial cycles, with increased productivity during interglacials and decreased productivity during glacials (*63*). This forms the basis of our stratigraphic alignment of the b* and diatom abundance with the Antarctic climate evolution across the last glacial–interglacial transition, as recorded by the δD of the EDC ice core (*3*).

Accordingly, we defined three tie points that link the major productivity increase and the included temporary productivity decrease reflected by the b* in core PC08 with the major deglacial Antarctic climate warming including the millennial-scale cooling during the ACR as reflected by the EDC δD (fig. S1). Another tie point marks the b*-based productivity decline corresponding to an Antarctic climate cooling after the early Holocene productivity and Antarctic temperature peak, while the core top is assumed to be recent. To constrain the glacial section in core PC08, where changes in b* and total diatom abundance are present but limited, we defined another two tie points also utilizing the magnetic susceptibility record. These glacial tie points mark productivity drops and increases in magnetic susceptibility reflecting increases in terrigenous sediment input related to downslope transport, ice rafted debris, and possibly dust, which are assumed to correspond to cooling transitions after millennial-scale Antarctic warm events in the EDC δD record (fig. S1). The resulting sedimentation rates for core site PC08 reveal values of 3.3 to 5.7 cm/ka for the late deglaciation and Holocene as compared to increased sedimentation rates of 8.7 to 9.6 cm/ka for the glacial and early deglaciation, consistent with an increased magnetic susceptibility reflecting enhanced

sediment deposition related to input of terrigenous detrital sediments (*27*, *28*).

The depth scale of core PC08 was placed on the Antarctic ice core chronology AICC2012 (*30*) based on the seven age-depth tie points (table S2) and using the R-Studio software and the "Bchronology" function in the "Bchron" package (*84*). Median ages (50% quantile) of the chronology are used for the age scale of PC08, while chronological uncertainty estimates are based on the age uncertainties of the tie points derived from the AICC2012 chronology. Six out of 10 AIOM ^{14}C ages calibrated with a reservoir age correction of either ΔR^{Hol} = 440 ± 80 years or ΔR^{CS} = 1600 ± 80 years are within the 2.5 and 97.5% quantiles and thus within the uncertainty of the tuning-based chronology of core PC08. Calibrated AIOM ^{14}C ages agree best with the tuning-based chronology and presumably are most reliable during the late deglaciation and early Holocene, probably related to an increased productivity (*83*). On the other hand, 4 out of 10 calibrated AIOM ^{14}C ages appear too old as compared with the tuning-based chronology of PC08, despite the additional reservoir age correction of ΔR^{CS} = 1600 ± 80 years. This is observed in intervals characterized by an increased magnetic susceptibility suggesting an enhanced input of reworked terrigenous sediment, particularly during the glacial and early deglaciation (fig. S1). A potential contribution of old organic matter (or dead carbon) from reworked sediments and/or an insufficient reservoir age correction likely biased the anomalously old AIOM ^{14}C ages (*83*).

Together, the tuning-based chronology suggests that the upper ~300 cm of core PC08 investigated in this study comprise the last ~40 ka and that the HBI biomarker records have a millennial-scale resolution. We acknowledge that the chronology might be flawed in parts, as the core top may not actually be recent and stratigraphic alignment in the glacial section is somewhat uncertain. Yet, the chronology of PC08 results in reasonable sedimentation rates and is overall consistent with independent AIOM ^{14}C-based age constraints. It is of particular importance for this study that the chronology appears robust especially for the deglaciation, where remarkably coherent changes in b* in core PC08 and δD of the EDC ice core enable a solid stratigraphic alignment that is verified by calibrated AIOM ^{14}C ages around the ACR.

Model simulations

The model output data used for the proxy-model data comparison in this study are based on a transient 140-ka experiment performed with the Earth system model of intermediate complexity, LOVECLIM (*85*). LOVECLIM is a coupled ocean–sea ice–atmosphere–vegetation model. The ocean–sea ice component consists of an ocean general circulation model with 3° × 3° resolution coupled to a thermodynamic-dynamic sea ice model with the same horizontal resolution. The atmospheric component is a spectral T21 model based on quasi-geostrophic equations. The transient model simulation is forced by time-dependent orbital parameters, ice sheet orography and surface albedo, and atmospheric greenhouse gases. Time- and latitude-dependent orbitally induced insolation changes were calculated according to Berger (*86*). The ice sheet boundary conditions were prescribed by changing ice-sheet orography and surface albedo, as derived from the time-dependent ice-sheet reconstruction as detailed by Menviel *et al.* (*87*) for the period 140 to 120 ka ago and by Abe-Ouchi *et al.* (*88*) for the past 120 ka. Varying atmospheric greenhouse gas concentrations were prescribed according to a smoothed compilation of greenhouse gas records from Antarctic ice cores (*89*). In addition, meltwater was added into the North Atlantic to simulate reductions of the AMOC associated with Heinrich events (fig. S4). The experiment was started at 140 ka ago following the PMIP4 protocol (*87*). The climatic evolution of the transient experiment presented here for the period 40 to 2 ka ago is similar to the one presented in Menviel *et al.* (*18*) and Menviel *et al.* (*24*), with small differences due to the different greenhouse gas and meltwater forcings.

For the proxy-model data comparison in this study, we extracted the simulated Austral summer (December-January-February) and annual mean sea ice concentration for core site PC08, which is averaged over 63°S to 65°S, 117°E to 123°E. In addition, we extracted the simulated Austral summer sea ice concentration for different latitudinal bands north of the core site, averaged over 60°S to 62°S, 117°E to 123°E and 58°S to 60°S, 117°E to 123°E.

Supplementary Materials

This PDF file includes:

Figs. S1 to S4
Tables S1 and S2
Legends for data S1 to S4
References

Other Supplementary Material for this manuscript includes the following:

Data S1 to S4

REFERENCES AND NOTES

1. E. Monnin, A. Indermühle, A. Dällenbach, J. Flückiger, B. Stauffer, T. F. Stocker, D. Raynaud, J.-M. Barnola, Atmospheric CO_2 concentrations over the last glacial termination. *Science* **291**, 112–114 (2001).
2. F. Parrenin, V. Masson-Delmotte, P. Köhler, D. Raynaud, D. Paillard, J. Schwander, C. Barbante, A. Landais, A. Wegner, J. Jouzel, Synchronous change of atmospheric CO_2 and Antarctic temperature during the last deglacial warming. *Science* **339**, 1060–1063 (2013).
3. J. Jouzel, V. Masson-Delmotte, O. Cattani, G. Dreyfus, S. Falourd, G. Hoffmann, B. Minster, J. Nouet, J. M. Barnola, J. Chappellaz, H. Fischer, J. C. Gallet, S. Johnsen, M. Leuenberger, L. Loulergue, D. Luethi, H. Oerter, F. Parrenin, G. Raisbeck, D. Raynaud, A. Schilt, J. Schwander, E. Selmo, R. Souchez, R. Spahni, B. Stauffer, J. P. Steffensen, B. Stenni, T. F. Stocker, J. L. Tison, M. Werner, E. W. Wolff, Orbital and millennial Antarctic climate variability over the past 800,000 years. *Science* **317**, 793–796 (2007).
4. C. Basak, H. Fröllje, F. Lamy, R. Gersonde, V. Benz, R. F. Anderson, M. Molina-Kescher, K. Pahnke, Breakup of last glacial deep stratification in the South Pacific. *Science* **359**, 900–904 (2018).
5. L. C. Skinner, S. Fallon, C. Waelbroeck, E. Michel, S. Barker, Ventilation of the deep Southern Ocean and deglacial CO_2 rise. *Science* **328**, 1147–1151 (2010).
6. R. F. Anderson, S. Ali, L. I. Bradtmiller, S. H. H. Nielsen, M. Q. Fleisher, B. E. Anderson, L. H. Burckle, Wind-driven upwelling in the Southern Ocean and the deglacial rise in atmospheric CO_2. *Science* **323**, 1443–1448 (2009).
7. G. H. Denton, R. F. Anderson, J. R. Toggweiler, R. L. Edwards, J. M. Schaefer, A. E. Putnam, The last glacial termination. *Science* **328**, 1652–1656 (2010).
8. D. J. Wilson, T. Struve, T. van de Flierdt, T. Chen, T. Li, A. Burke, L. F. Robinson, Sea-ice control on deglacial lower cell circulation changes recorded by Drake Passage deep-sea corals. *Earth Planet. Sci. Lett.* **544**, 116405 (2020).
9. R. Ferrari, M. F. Jansen, J. F. Adkins, A. Burke, A. L. Stewart, A. F. Thompson, Antarctic sea ice control on ocean circulation in present and glacial climates. *Proc. Natl. Acad. Sci. U.S.A.* **111**, 8753–8758 (2014).
10. L.-P. Nadeau, R. Ferrari, M. F. Jansen, Antarctic sea ice control on the depth of North Atlantic deep water. *J. Climate* **32**, 2537–2551 (2019).
11. B. B. Stephens, R. F. Keeling, The influence of Antarctic sea ice on glacial-interglacial CO_2 variations. *Nature* **404**, 171–174 (2000).
12. S. Barker, P. Diz, M. J. Vautravers, J. Pike, G. Knorr, I. R. Hall, W. S. Broecker, Interhemispheric Atlantic seesaw response during the last deglaciation. *Nature* **457**, 1097–1102 (2009).

13. S. O. Rasmussen, M. Bigler, S. P. Blockley, T. Blunier, S. L. Buchardt, H. B. Clausen, I. Cvijanovic, D. Dahl-Jensen, S. J. Johnsen, H. Fischer, V. Gkinis, M. Guillevic, W. Z. Hoek, J. J. Lowe, J. B. Pedro, T. Popp, I. K. Seierstad, J. P. Steffensen, A. M. Svensson, P. Vallelonga, B. M. Vinther, M. J. C. Walker, J. J. Wheatley, M. Winstrup, A stratigraphic framework for abrupt climatic changes during the Last Glacial period based on three synchronized Greenland ice-core records: Refining and extending the INTIMATE event stratigraphy. *Quat. Sci. Rev.* **106**, 14–28 (2014).
14. J. F. McManus, R. Francois, J. M. Gherardi, L. D. Keigwin, S. Brown-Leger, Collapse and rapid resumption of Atlantic meridional circulation linked to deglacial climate changes. *Nature* **428**, 834–837 (2004).
15. T. F. Stocker, S. J. Johnsen, A minimum thermodynamic model for the bipolar seesaw. *Paleoceanography* **18**, 1087 (2003).
16. J. Gottschalk, G. Battaglia, H. Fischer, T. L. Frölicher, S. L. Jaccard, A. Jeltsch-Thömmes, F. Joos, P. Köhler, K. J. Meissner, L. Menviel, C. Nehrbass-Ahles, J. Schmitt, A. Schmittner, L. C. Skinner, T. F. Stocker, Mechanisms of millennial-scale atmospheric CO_2 change in numerical model simulations. *Quat. Sci. Rev.* **220**, 30–74 (2019).
17. J. B. Pedro, H. C. Bostock, C. M. Bitz, F. He, M. J. Vandergoes, E. J. Steig, B. M. Chase, C. E. Krause, S. O. Rasmussen, B. R. Markle, G. Cortese, The spatial extent and dynamics of the Antarctic Cold Reversal. *Nat. Geosci.* **9**, 51–55 (2016).
18. L. Menviel, A. Timmermann, O. E. Timm, A. Mouchet, Deconstructing the Last Glacial termination: The role of millennial and orbital-scale forcings. *Quat. Sci. Rev.* **30**, 1155–1172 (2011).
19. WAIS Divide Project Members, Onset of deglacial warming in West Antarctica driven by local orbital forcing. *Nature* **500**, 440–444 (2013).
20. T. A. Ronge, J. Lippold, W. Geibert, S. L. Jaccard, S. Mieruch-Schnülle, F. Süfke, R. Tiedemann, Deglacial patterns of South Pacific overturning inferred from ^{231}Pa and ^{230}Th. *Sci. Rep.* **11**, 20473 (2021).
21. X. Crosta, K. E. Kohfeld, H. C. Bostock, M. Chadwick, A. Du Vivier, O. Esper, J. Etourneau, J. Jones, A. Leventer, J. Müller, R. H. Rhodes, C. S. Allen, P. Ghadi, N. Lamping, C. B. Lange, K.-A. Lawler, D. Lund, A. Marzocchi, K. J. Meissner, L. Menviel, A. Nair, M. Patterson, J. Pike, J. G. Prebble, C. Riesselman, H. Sadatzki, L. C. Sime, S. K. Shukla, L. Thöle, M.-E. Vorrath, W. Xiao, J. Yang, Antarctic sea ice over the past 130,000 years—Part 1: A review of what proxy records tell us. *Clim. Past* **18**, 1729–1756 (2022).
22. M. Chadwick, X. Crosta, O. Esper, L. Thöle, K. E. Kohfeld, Compilation of Southern Ocean sea-ice records covering the last glacial-interglacial cycle (12–130 ka). *Clim. Past* **18**, 1815–1829 (2022).
23. R. Gersonde, U. Zielinski, The reconstruction of late Quaternary Antarctic sea-ice distribution—The use of diatoms as a proxy for sea-ice. *Palaeogeogr. Palaeoclimatol. Palaeoecol.* **162**, 263–286 (2000).
24. L. Menviel, A. Timmermann, T. Friedrich, M. H. England, Hindcasting the continuum of Dansgaard-Oeschger variability: Mechanisms, patterns and timing. *Clim. Past* **10**, 63–77 (2014).
25. L. K. Armand, P. E. O'Brien, On-board Scientific Party, Interactions of the Totten Glacier with the Southern Ocean through multiple glacial cycles (IN2017-V01): Post-survey report. Research School of Earth Sciences, Australian National University, Canberra, https://doi.org/10.4225/13/5acea64c48693 (2018).
26. T. Tamura, K. I. Ohshima, S. Nihashi, Mapping of sea ice production for Antarctic coastal polynyas. *Geophys. Res. Lett.* **35**, L07606 (2008).
27. L. Holder, M. Duffy, B. Opdyke, A. Leventer, A. Post, P. O'Brien, L. K. Armand, Controls since the mid-Pleistocene transition on sedimentation and primary productivity downslope of Totten Glacier, East Antarctica. *Paleoceanogr. Paleoclimatol.* **35**, e2020PA003981 (2020).
28. S. Tooze, J. A. Halpin, T. L. Noble, Z. Chase, P. E. O'Brien, L. Armand, Scratching the surface: A marine sediment provenance record from the continental slope of central Wilkes Land, East Antarctica. *Geochem. Geophys. Geosyst.* **21**, e2020GC009156 (2020).
29. D. Sprenk, M. E. Weber, G. Kuhn, P. Rosén, M. Frank, M. Molina-Kescher, V. Liebetrau, H.-G. Röhling, Southern Ocean bioproductivity during the last glacial cycle—New detection method and decadal-scale insight from the Scotia Sea. *Geol. Soc. Lond. Spec. Publ.* **381**, 245–261 (2013).
30. D. Veres, L. Bazin, A. Landais, H. T. M. Kele, B. Lemieux-Dudon, F. Parrenin, P. Martinerie, E. Blayo, T. Blunier, E. Capron, J. Chappellaz, S. O. Rasmussen, M. Severi, A. Svensson, B. Vinther, E. W. Wolff, The Antarctic ice core chronology (AICC2012): An optimized multi-parameter and multi-site dating approach for the last 120 thousand years. *Clim. Past* **9**, 1733–1748 (2013).
31. J. Fenner, Eocene-Oligocene planktic diatom stratigraphy in the low latitudes and the high southern latitudes. *Micropaleontology* **30**, 319–342 (1984).
32. P. E. O'Brien, A. L. Post, S. Edwards, T. Martin, A. Caburlotto, F. Donda, G. Leitchenkov, R. Romero, M. Duffy, D. Evangelinos, L. Holder, A. Leventer, A. López-Quirós, B. N. Opdyke, L. K. Armand, Continental slope and rise geomorphology seaward of the Totten Glacier, East Antarctica (112°E-122°E). *Mar. Geol.* **427**, 106221 (2020).
33. G. Massé, S. T. Belt, X. Crosta, S. Schmidt, I. Snape, D. N. Thomas, S. J. Rowland, Highly branched isoprenoids as proxies for variable sea ice conditions in the Southern Ocean. *Antarct. Sci.* **23**, 487–498 (2011).
34. S. T. Belt, L. Smik, T. A. Brown, J.-H. Kim, S. J. Rowland, C. S. Allen, J.-K. Gal, K.-H. Shin, J. I. Lee, K. W. R. Taylor, Source identification and distribution reveals the potential of the geochemical Antarctic sea ice proxy $IPSO_{25}$. *Nat. Commun.* **7**, 12655 (2016).
35. S. T. Belt, Source-specific biomarkers as proxies for Arctic and Antarctic sea ice. *Org. Geochem.* **125**, 277–298 (2018).
36. L. Smik, S. T. Belt, J. L. Lieser, L. K. Armand, A. Leventer, Distributions of highly branched isoprenoid alkenes and other algal lipids in surface waters from East Antarctica: Further insights for biomarker-based paleo sea-ice reconstruction. *Org. Geochem.* **95**, 71–80 (2016).
37. M.-E. Vorrath, J. Müller, O. Esper, G. Mollenhauer, C. Haas, E. Schefuß, K. Fahl, Highly branched isoprenoids for Southern Ocean sea ice reconstructions: A pilot study from the Western Antarctic Peninsula. *Biogeosciences* **16**, 2961–2981 (2019).
38. J. Müller, A. Wagner, K. Fahl, R. Stein, M. Prange, G. Lohmann, Towards quantitative sea ice reconstructions in the northern North Atlantic: A combined biomarker and numerical modelling approach. *Earth Planet. Sci. Lett.* **306**, 137–148 (2011).
39. N. Lamping, J. Müller, J. Hefter, G. Mollenhauer, C. Haas, X. Shi, M.-E. Vorrath, G. Lohmann, C.-D. Hillenbrand, Evaluation of lipid biomarkers as proxies for sea ice and ocean temperatures along the Antarctic continental margin. *Clim. Past* **17**, 2305–2326 (2021).
40. L. K. Armand, X. Crosta, O. Romero, J.-J. Pichon, The biogeography of major diatom taxa in Southern Ocean sediments: 1. Sea ice related species. *Palaeogeogr. Palaeoclimatol. Palaeoecol.* **223**, 93–126 (2005).
41. X. Crosta, J. Etourneau, L. C. Orme, Q. Dalaiden, P. Campagne, D. Swingedouw, H. Goosse, G. Massé, A. Miettinen, R. M. McKay, R. B. Dunbar, C. Escutia, M. Ikehara, Multi-decadal trends in Antarctic sea-ice extent driven by ENSO–SAM over the last 2,000 years. *Nat. Geosci.* **14**, 156–160 (2021).
42. W. S. Xiao, O. Esper, R. Gersonde, Last Glacial–Holocene climate variability in the Atlantic sector of the Southern Ocean. *Quat. Sci. Rev.* **135**, 115–137 (2016).
43. A. J. Ferry, X. Crosta, P. G. Quilty, D. Fink, W. Howard, L. K. Armand, First records of winter sea ice concentration in the southwest Pacific sector of the Southern Ocean. *Paleoceanography* **30**, 1525–1539 (2015).
44. J. Jones, K. E. Kohfeld, H. Bostock, X. Crosta, M. Liston, G. Dunbar, Z. Chase, A. Leventer, H. Anderson, G. Jacobsen, Sea ice changes in the southwest Pacific sector of the Southern Ocean during the last 140,000 years. *Clim. Past* **18**, 465–483 (2022).
45. X. Crosta, A. Sturm, L. Armand, J.-J. Pichon, Late Quaternary sea ice history in the Indian sector of the Southern Ocean as recorded by diatom assemblages. *Mar. Micropaleontol.* **50**, 209–223 (2004).
46. R. Gersonde, X. Crosta, A. Abelmann, L. Armand, Sea-surface temperature and sea ice distribution of the Southern Ocean at the EPILOG Last Glacial Maximum—A circum-Antarctic view based on siliceous microfossil records. *Quat. Sci. Rev.* **24**, 869–896 (2005).
47. L. G. Collins, J. Pike, C. S. Allen, D. A. Hodgson, High-resolution reconstruction of southwest Atlantic sea-ice and its role in the carbon cycle during marine isotope stages 3 and 2. *Paleoceanography* **27**, PA3217 (2012).
48. C. S. Allen, J. Pike, C. J. Pudsey, Last glacial–interglacial sea-ice cover in the SW Atlantic and its potential role in global deglaciation. *Quat. Sci. Rev.* **30**, 2446–2458 (2011).
49. A. Shemesh, D. Hodell, X. Crosta, S. Kanfoush, C. Charles, T. Guilderson, Sequence of events during the last deglaciation in Southern Ocean sediments and Antarctic ice cores. *Paleoceanography* **17**, 8-1–8-7 (2002).
50. R. A. Green, L. Menviel, K. Meissner, X. Crosta, D. Chandan, G. Lohmann, W. R. Peltier, X. Shi, J. Zhu, Evaluating seasonal sea-ice cover over the Southern Ocean at the Last Glacial Maximum. *Clim. Past* **18**, 845–862 (2022).
51. E. W. Wolff, H. Fischer, F. Fundel, U. Ruth, B. Twarloh, G. C. Littot, R. Mulvaney, R. Röthlisberger, M. de Angelis, C. F. Boutron, M. Hansson, U. Jonsell, M. A. Hutterli, F. Lambert, P. Kaufmann, B. Stauffer, T. F. Stocker, J. P. Steffensen, M. Bigler, M. L. Siggaard-Andersen, R. Udisti, S. Becagli, E. Castellano, M. Severi, D. Wagenbach, C. Barbante, P. Gabrielli, V. Gaspari, Southern Ocean sea-ice extent, productivity and iron flux over the past eight glacial cycles. *Nature* **440**, 491–496 (2006).
52. H. Fischer, F. Fundel, U. Ruth, B. Twarloh, A. Wegner, R. Udisti, S. Becagli, E. Castellano, A. Morganti, M. Severi, E. Wolff, G. Littot, R. Röthlisberger, R. Mulvaney, M. A. Hutterli, P. Kaufmann, U. Federer, F. Lambert, M. Bigler, M. Hansson, U. Jonsell, M. de Angelis, C. Boutron, M.-L. Siggaard-Andersen, J. P. Steffensen, C. Barbante, V. Gaspari, P. Gabrielli, D. Wagenbach, Reconstruction of millennial changes in dust emission, transport and regional sea ice coverage using the deep EPICA ice cores from the Atlantic and Indian Ocean sector of Antarctica. *Earth Planet. Sci. Lett.* **260**, 340–354 (2007).
53. P. De Deckker, M. Moros, K. Perner, E. Jansen, Influence of the tropics and southern westerlies on glacial interhemispheric asymmetry. *Nat. Geosci.* **5**, 266–269 (2012).

54. P. De Deckker, M. Moros, K. Perner, T. Blanz, L. Wacker, R. Schneider, T. T. Barrows, T. O'Loingsigh, E. Jansen, Climatic evolution in the Australian region over the last 94 ka - spanning human occupancy -, and unveiling the Last Glacial Maximum. *Quat. Sci. Rev.* **249**, 106593 (2020).
55. P. Huybers, G. Denton, Antarctic temperature at orbital timescales controlled by local summer duration. *Nat. Geosci.* **1**, 787–792 (2008).
56. A. Timmermann, O. Timm, L. Stott, L. Menviel, The roles of CO_2 and orbital forcing in driving Southern Hemispheric temperature variations during the last 21 000 yr. *J. Clim.* **22**, 1626–1640 (2009).
57. P. Huybers, Early Pleistocene glacial cycles and the integrated summer insolation forcing. *Science* **313**, 508–511 (2006).
58. G. Ménot, E. Bard, F. Rostek, J. W. H. Weijers, E. C. Hopmans, S. Schouten, J. S. Sinninghe Damsté, Early reactivation of European rivers during the last deglaciation. *Science* **313**, 1623–1625 (2006).
59. V. L. Peck, I. R. Hall, R. Zahn, H. Elderfield, F. Grousset, S. R. Hemming, J. D. Scourse, High resolution evidence for linkages between NW European ice sheet instability and Atlantic meridional overturning circulation. *Earth Planet. Sci. Lett.* **243**, 476–488 (2006).
60. A. D. Moy, W. R. Howard, M. K. Gagan, Late Quaternary palaeoceanography of the Circumpolar Deep Water from the South Tasman Rise. *J. Quat. Sci.* **21**, 763–777 (2006).
61. J. R. Toggweiler, J. L. Russell, S. R. Carson, Midlatitude westerlies, atmospheric CO_2, and climate change during the ice ages. *Paleoceanography* **21**, PA2005 (2006).
62. L. Menviel, P. Spence, J. Yu, M. A. Chamberlain, R. J. Matear, K. J. Meissner, M. H. England, Southern Hemisphere westerlies as a driver of the early deglacial atmospheric CO_2 rise. *Nat. Commun.* **9**, 2503 (2018).
63. L. Lu, X. Zheng, Z. Chen, W. Yan, S. Wu, L.-W. Zheng, X. Wang, Y. Chen, S. Kao, One-to-one coupling between Southern Ocean productivity and Antarctica climate. *Geophys. Res. Lett.* **49**, e2022GL098761 (2022).
64. D. M. Sigman, E. A. Boyle, Glacial/interglacial variations in atmospheric carbon dioxide. *Nature* **407**, 859–869 (2000).
65. T. Li, L. F. Robinson, T. Chen, X. T. Wang, A. Burke, J. W. B. Rae, A. Pegrum-Haram, T. D. J. Knowles, G. Li, J. Chen, H. Chin Ng, M. Prokopenko, G. H. Rowland, A. Samperiz, J. A. Stewart, J. Southon, P. T. Spooner, Rapid shifts in circulation and biogeochemistry of the Southern Ocean during deglacial carbon cycle events. *Sci. Adv.* **6**, eabb3807 (2020).
66. J. Gottschalk, E. Michel, L. M. Thöle, A. S. Studer, A. P. Hasenfratz, N. Schmid, M. Butzin, A. Mazaud, A. Martínez-García, S. Szidat, S. L. Jaccard, Glacial heterogeneity in Southern Ocean carbon storage abated by fast South Indian deglacial carbon release. *Nat. Commun.* **11**, 6192 (2020).
67. J. W. B. Rae, A. Burke, L. F. Robinson, J. F. Adkins, T. Chen, C. Cole, R. Greenop, T. Li, E. F. M. Littley, D. C. Nita, J. A. Stewart, B. J. Taylor, CO_2 storage and release in the deep Southern Ocean on millennial to centennial timescales. *Nature* **562**, 569–573 (2018).
68. J. Schmitt, R. Schneider, J. Elsig, D. Leuenberger, A. Lourantou, J. Chappellaz, P. Köhler, F. Joos, T. F. Stocker, M. Leuenberger, H. Fischer, Carbon isotope constraints on the deglacial CO_2 rise from ice cores. *Science* **336**, 711–714 (2012).
69. T. K. Bauska, D. Baggenstos, E. J. Brook, A. C. Mix, S. A. Marcott, V. V. Petrenko, H. Schaefer, J. P. Severinghaus, J. E. Lee, Carbon isotopes characterize rapid changes in atmospheric carbon dioxide during the last deglaciation. *Proc. Natl. Acad. Sci. U.S.A.* **113**, 3465–3470 (2016).
70. S. A. Marcott, T. K. Bauska, C. Buizert, E. J. Steig, J. L. Rosen, K. M. Cuffey, T. J. Fudge, J. P. Severinghaus, J. Ahn, M. L. Kalk, J. R. McConnell, T. Sowers, K. C. Taylor, J. W. C. White, E. J. Brook, Centennial-scale changes in the global carbon cycle during the last deglaciation. *Nature* **514**, 616–619 (2014).
71. J. P. Warnock, R. P. Scherer, A revised method for determining the absolute abundance of diatoms. *J. Paleolimnol.* **53**, 157–163 (2015).
72. A. O. Cefarelli, M. E. Ferrario, G. O. Almandoz, A. G. Atencio, R. Akselman, M. Vernet, Diversity of the diatom genus *Fragilariopsis* in the Argentine Sea and Antarctic waters: Morphology, distribution and abundance. *Polar Biol.* **33**, 1463–1484 (2010).
73. X. Crosta, O. Romero, L. K. Armand, J.-J. Pichon, The biogeography of major diatom taxa in Southern Ocean sediments: 2. Open ocean related species. *Palaeogeogr. Palaeoclimatol. Palaeoecol.* **223**, 66–92 (2005).
74. S. T. Belt, T. A. Brown, L. Ampel, P. Cabedo-Sanz, K. Fahl, J. J. Kocis, G. Massé, A. Navarro-Rodriguez, J. Ruan, Y. Xu, An inter-laboratory investigation of the Arctic sea ice biomarker proxy IP_{25} in marine sediments: Key outcomes and recommendations. *Clim. Past* **10**, 155–166 (2014).
75. S. T. Belt, P. Cabedo-Sanz, L. Smik, A. Navarro-Rodriguez, S. M. P. Berben, J. Knies, K. Husum, Identification of paleo Arctic winter sea ice limits and the marginal ice zone: Optimised biomarker-based reconstructions of late Quaternary Arctic sea ice. *Earth Planet. Sci. Lett.* **431**, 127–139 (2015).
76. J. J. Brocks, J. M. Hope, Tailing of chromatographic peaks in GC-MS caused by interaction of halogenated solvents with the ion source. *J. Chromatogr. Sci.* **52**, 471–475 (2014).
77. S. T. Belt, W. G. Allard, G. Massé, J.-M. Robert, S. J. Rowland, Highly branched isoprenoids (HBIs): Identification of the most common and abundant sedimentary isomers. *Geochim. Cosmochim. Acta* **64**, 3839–3851 (2000).
78. M. Stuiver, H. A. Polach, Discussion reporting of ^{14}C data. *Radiocarbon* **19**, 355–363 (1977).
79. M. Stuiver, P. J. Reimer, R. W. Reimer, 2022. CALIB 8.2 [WWW program], http://calib.org [accessed 15 March 2022].
80. T. J. Heaton, P. Köhler, M. Butzin, E. Bard, R. W. Reimer, W. E. N. Austin, C. Bronk Ramsey, P. M. Grootes, K. A. Hughen, B. Kromer, P. J. Reimer, J. Adkins, A. Burke, M. S. Cook, J. Olsen, L. C. Skinner, Marine20—The marine radiocarbon age calibration curve (0–55,000 cal BP). *Radiocarbon* **62**, 779–820 (2020).
81. T. J. Heaton, M. Butzin, E. Bard, C. Bronk Ramsey, K. A. Hughen, P. Köhler, P. J. Reimer, Marine radiocarbon calibration in polar regions: A simple approximate approach using Marine20. *Radiocarbon*, 1–28 (2023). https://doi.org/10.1017/RDC.2023.42.
82. M. Paterne, E. Michel, V. Héros, Variability of marine ^{14}C reservoir ages in the Southern Ocean highlighting circulation changes between 1910 and 1950. *Earth Planet. Sci. Lett.* **511**, 99–104 (2019).
83. K. J. Licht, W. L. Cunningham, J. T. Andrews, E. W. Domack, A. E. Jennings, Establishing chronologies from acid-insoluble organic 14C dates on Antarctic (Ross Sea) and Arctic (North Atlantic) marine sediments. *Polar Res.* **17**, 203–216 (1998).
84. J. Haslett, A. Parnell, A simple monotone process with application to radiocarbon-dated depth chronologies. *J. R. Stat. Soc. Ser. C* **57**, 399–418 (2008).
85. H. Goosse, V. Brovkin, T. Fichefet, R. Haarsma, P. Huybrechts, J. Jongma, A. Mouchet, F. Selten, P.-Y. Barriat, J.-M. Campin, E. Deleersnijder, E. Driesschaert, H. Goelzer, I. Janssens, M.-F. Loutre, M. A. Morales Maqueda, T. Opsteegh, P.-P. Mathieu, G. Munhoven, E. J. Pettersson, H. Renssen, D. M. Roche, M. Schaeffer, B. Tartinville, A. Timmermann, S. L. Weber, Description of the Earth system model of intermediate complexity LOVECLIM version 1.2. *Geosci. Model Dev.* **3**, 603–633 (2010).
86. A. Berger, Long-term variations of caloric insolation resulting from the earth's orbital elements. *Quatern. Res.* **9**, 139–167 (1978).
87. L. Menviel, E. Capron, A. Govin, A. Dutton, L. Tarasov, A. Abe-Ouchi, R. N. Drysdale, P. L. Gibbard, L. Gregoire, F. He, R. F. Ivanovic, M. Kageyama, K. Kawamura, A. Landais, B. L. Otto-Bliesner, I. Oyabu, P. C. Tzedakis, E. Wolff, X. Zhang, The penultimate deglaciation: Protocol for Paleoclimate Modelling Intercomparison Project (PMIP) phase 4 transient numerical simulations between 140 and 127 ka, version 1.0. *Geosci. Model Dev.* **12**, 3649–3685 (2019).
88. A. Abe-Ouchi, F. Saito, K. Kawamura, M. E. Raymo, J. Okuno, K. Takahashi, H. Blatter, Insolation-driven 100,000-year glacial cycles and hysteresis of ice-sheet volume. *Nature* **500**, 190–193 (2013).
89. P. Köhler, C. Nehrbass-Ahles, J. Schmitt, T. F. Stocker, H. Fischer, A 156 kyr smoothed history of the atmospheric greenhouse gases CO_2, CH_4, and N_2O and their radiative forcing. *Earth Syst. Sci. Data* **9**, 363–387 (2017).
90. F. Fetterer, K. Knowles, W. Meier, M. Savoie, A. K. Windnagel, *Sea Ice Index, Version 3* (NSIDC National Snow Ice Data Center, 2017).
91. A. H. Orsi, T. Whitworth, W. D. Nowlin, On the meridional extent and fronts of the Antarctic Circumpolar Current. *Deep Sea Res.* **42**, 641–673 (1995).
92. R. Schlitzer, Ocean Data View (2017). https://odv.awi.de/ [accessed 6 February 2017].
93. P. U. Clark, A. S. Dyke, J. D. Shakun, A. E. Carlson, J. Clark, B. Wohlfarth, J. X. Mitrovica, S. W. Hostetler, A. Marshall McCabe, The Last Glacial Maximum. *Science* **325**, 710–714 (2009).
94. WAIS Divide Project Members, Precise interpolar phasing of abrupt climate change during the last ice age. *Nature* **520**, 661–665 (2015).
95. C. Buizert, K. M. Cuffey, J. P. Severinghaus, D. Baggenstos, T. J. Fudge, E. J. Steig, B. R. Markle, M. Winstrup, R. H. Rhodes, E. J. Brook, T. A. Sowers, G. D. Clow, H. Cheng, R. L. Edwards, M. Sigl, J. R. McConnell, K. C. Taylor, The WAIS Divide deep ice core WD2014 chronology. Part 1. Methane synchronization (68–31 ka BP) and the gas age–ice age difference. *Clim. Past.* **11**, 153–173 (2015).
96. P. J. Huybers, (2006-08-24): *NOAA/WDS Paleoclimatology–Huybers 2006 Integrated Summer Insolation Forcing Data*. [j_65south.txt]. NOAA National Centers for Environmental Information, https://doi.org/10.25921/nv5w-rh04 [accessed 31 March 2020].
97. J. Laskar, P. Robutel, F. Joutel, M. Gastineau, A. C. M. Correia, B. Levrard, A long-term numerical solution for the insolation quantities of the Earth. *Astron. Astrophys.* **428**, 261–285 (2004).
98. A. D. Moy, M. R. Palmer, W. R. Howard, J. Bijma, M. J. Cooper, E. Calvo, C. Pelejero, M. K. Gagan, T. B. Chalk, Varied contribution of the Southern Ocean to deglacial atmospheric CO_2 rise. *Nat. Geosci.* **12**, 1006–1011 (2019).
99. S. Eggleston, J. Schmitt, B. Bereiter, R. Schneider, H. Fischer, Evolution of the stable carbon isotope composition of atmospheric CO_2 over the last glacial cycle. *Paleoceanography* **31**, 434–452 (2016).

100. J. Lippold, J. Grützner, D. Winter, Y. Lahaye, A. Mangini, M. Christl, Does sedimentary $^{231}Pa/^{230}Th$ from the Bermuda Rise monitor past Atlantic Meridional Overturning Circulation? *Geophys. Res. Lett.* **36**, L12601 (2009).

Acknowledgments: We thank the Marine National Facility, the IN2017-V01 scientific party led by the Chief Scientists L.K. Armand and P. O'Brien, MNF support staff, and ASP crew members led by M. Watson for their help and support on board the RV *Investigator*. We wish to thank the CSIRO MNF for its support in the form of sea time on RV *Investigator*, support personnel, scientific equipment, and data management. All data and samples acquired on the voyage are made publicly available in accordance with MNF Policy. We are grateful to S. Belt and L. Smik for providing the internal standard 9-OHD and reference sediment material for HBI analysis, to A. Moy for providing the data of core MD97-2106 on the latest chronology, and to K.-A. Lawler for helping with sample processing for AIOM ^{14}C analysis. **Funding:** This project is supported through funding from the Australian Government's Australian Antarctic Science Grant Program (AAS #4333). This research was funded by the Australian Government through the Australian Research Council (DP170100557). This research was supported by the Australian Research Council Special Research Initiative, Australian Centre for Excellence in Antarctic Science (Project Number SR200100008). L.M. acknowledges funding from the Australian Research Council FT180100606. The LOVECLIM experiment was performed on the UNSW HPC cluster Katana supported by Research Technology Services at UNSW Sydney. We acknowledge support by the Open Access Publication Funds of Alfred-Wegener-Institut Helmholtz-Zentrum für Polar- und Meeresforschung. **Author contributions:** Conceptualization: H.S., B.O., L.M., and L.A. Methodology: H.S., B.O., L.M., A.L., J.M.H., J.J.B., S.F., A.L.P., P.E.O., and K.G. Investigation: H.S., B.O., and L.M.. Visualization: H.S. and L.M. Supervision: H.S. and L.A. Writing—original draft: H.S., L.M., J.M.H., J.J.B., and S.F. Writing—review and editing: H.S., B.O., L.M., A.L., J.M.H., J.J.B., S.F., A.L.P., P.E.O., and K.G. **Competing interests:** The authors declare that they have no competing interests. **Data and materials availability:** All data needed to evaluate the conclusions in the paper are present in the paper and/or the Supplementary Materials. Sediment core proxy data and model output data reported in this study are available in the other Supplementary Materials accompanying this paper.

Submitted 24 March 2023
Accepted 7 September 2023
Published 12 October 2023
10.1126/sciadv.adh9513

ScienceAdvances

Early sea ice decline off East Antarctica at the last glacial–interglacial climate transition

Henrik Sadatzki, Bradley Opdyke, Laurie Menviel, Amy Leventer, Janet M. Hope, Jochen J. Brocks, Stewart Fallon, Alexandra L. Post, Philip E. O'Brien, Katharine Grant, and Leanne Armand

Sci. Adv. **9** (41), eadh9513. DOI: 10.1126/sciadv.adh9513